Single-molecule analysis reveals human UV-damaged DNA-binding protein (UV-DDB) dimerizes on DNA via multiple kinetic intermediates

Harshad Ghodke[a,b], Hong Wang[c], Ching L. Hsieh[b,d], Selamawit Woldemeskel[a], Simon C. Watkins[e], Vesna Rapić-Otrin[b,d], and Bennett Van Houten[a,b,1]

[a]Department of Pharmacology and Chemical Biology, University of Pittsburgh School of Medicine, Pittsburgh, PA 15213; [b]University of Pittsburgh Cancer Institute, Pittsburgh, PA 15213; [c]Department of Physics, North Carolina State University, Raleigh, NC 27695; [d]Department of Microbiology and Molecular Genetics, University of Pittsburgh School of Medicine, Pittsburgh, PA 15213; and [e]Center for Biologic Imaging, University of Pittsburgh School of Medicine, Pittsburgh, PA 15261

Edited by Graham C. Walker, Massachusetts Institute of Technology, Cambridge, MA, and approved March 17, 2014 (received for review December 21, 2013)

How human DNA repair proteins survey the genome for UV-induced photoproducts remains a poorly understood aspect of the initial damage recognition step in nucleotide excision repair (NER). To understand this process, we performed single-molecule experiments, which revealed that the human UV-damaged DNA-binding protein (UV-DDB) performs a 3D search mechanism and displays a remarkable heterogeneity in the kinetics of damage recognition. Our results indicate that UV-DDB examines sites on DNA in discrete steps before forming long-lived, nonmotile UV-DDB dimers $(DDB1\text{-}DDB2)_2$ at sites of damage. Analysis of the rates of dissociation for the transient binding molecules on both undamaged and damaged DNA show multiple dwell times over three orders of magnitude: 0.3–0.8, 8.1, and 113–126 s. These intermediate states are believed to represent discrete UV-DDB conformers on the trajectory to stable damage detection. DNA damage promoted the formation of highly stable dimers lasting for at least 15 min. The xeroderma pigmentosum group E (XP-E) causing K244E mutant of DDB2 found in patient XP82TO, supported UV-DDB dimerization but was found to slide on DNA and failed to stably engage lesions. These findings provide molecular insight into the loss of damage discrimination observed in this XP-E patient. This study proposes that UV-DDB recognizes lesions via multiple kinetic intermediates, through a conformational proofreading mechanism.

DNA damage recognition | single-molecule tracking | DNA tightrope | human nucleotide excision repair

Unrepaired photoproducts in the genome arising from exposure to UV irradiation can be highly mutagenic and three pathways have evolved in mammalian cells to process these lesions, which include (*i*) global genomic repair, (*ii*) transcription-coupled repair, and (*iii*) translesion synthesis (1–5). During global genomic repair, cyclobutane pyrimidine dimers (CPDs) and pyrimidine(6–4)pyrimidone photoproducts [(6–4) photoproducts] are repaired by the nucleotide excision repair (NER) pathway that recognizes and excises bulky helix distorting lesions in the genome (6, 7). The recognition of CPD lesions in UV-damaged chromatin is mediated by UV-damaged DNA-binding protein (UV-DDB), composed of the tightly associated heterodimer of damage-specific DNA binding protein (DDB) 1 (p127) and DDB2 (p48) (5, 8). Following surveillance and CPD identification by UV-DDB, NER proceeds via lesion handover to XPC–hHR23B–centrin2 (XPC) followed by damage verification, helix opening and stabilizing of the repair intermediates, dual incision of the DNA in the context of the lesion, repair synthesis, and DNA ligation (7). In contrast to global genomic repair, transcription-coupled repair is initiated when CPD lesions in transcribed chromatin cause stalling of RNA polymerases (3). In mammalian NER, these two pathways converge after damage detection and are orchestrated by over 30 different gene products (9). Deficiencies in the molecular functions in seven of these NER proteins lead to various forms of the autosomal recessive disorder termed xeroderma pigmentosum (XP) (10). Finally, unrepaired, CPDs can be bypassed during DNA replication by specialized DNA polymerases, such as DNA polymerase η (pol η) (2). Mutations in the gene encoding pol η give rise to the eighth complementation group of XP, the XP variant phenotype.

Molecular defects in DDB2 lead to a slower loss of UV-induced photoproducts and presentation of the skin cancer prone XP complementation group E (XP-E) (11, 12). Recombinant DDB2 has been demonstrated to bind a variety of DNA structures including 6–4 photoproducts, abasic sites, and two base mismatches with remarkably high affinity and CPD lesions and cisplatin adducts with relatively lower affinity (13–15). Molecular analysis of XP-E patients revealed genetic defects in the DDB2 gene, which give rise to truncations, misfolding, or a modification of the DNA-binding interface of DDB2 (11, 12). In the case of the XP82TO patient, a lysine-to-glutamate point mutation at position 244 (K244E) was observed in DDB2, which results in significantly reduced DNA-binding activity and specificity for damage (11, 12).

In vivo, UV-DDB is constitutively associated with Cullin4A or 4B and RBX1, forming the $CRL4^{DDB2}$ E3 ligase complex (16–18). In this complex, DDB2 is a DNA damage-recognition factor and functions as an adapter protein which targets the E3 ligase activity to sites of UV-induced photoproducts, promoting

Significance

UV damage in genomic DNA is identified by the human UV-damaged DNA-binding protein (UV-DDB). Recognition of DNA damage by UV-DDB serves to initiate global genomic nucleotide excision repair (NER) in humans. Recent work has revealed that UV-DDB dimerizes at sites of damage. This study demonstrates that prior to stable damage recognition, UV-DDB interrogates DNA for damage via a 3D diffusion mechanism coupled to the formation of multiple transient intermediates. Stable binding at sites of damage is achieved by dimerization of UV-DDB. This study also analyzed a disease-causing mutant of UV-DDB, which was found to slide on DNA, while retaining the ability to dimerize on DNA. These results enhance our understanding of damage recognition in NER in humans.

Author contributions: H.G., V.R.-O., and B.V.H. designed research; H.G. and S.W. performed research; H.W., C.L.H., and S.C.W. contributed new reagents/analytic tools; H.G. and B.V.H. analyzed data; and H.G., V.R.-O., and B.V.H. wrote the paper.

The authors declare no conflict of interest.

This article is a PNAS Direct Submission.

Freely available online through the PNAS open access option.

[1]To whom correspondence should be addressed. E-mail: vanhoutenb@upmc.edu.

This article contains supporting information online at www.pnas.org/lookup/suppl/doi:10.1073/pnas.1323856111/-/DCSupplemental.

chromatin relaxation, and enabling access to subsequent repair factors (14, 18–20). A current working model for damage recognition in global genomic repair is that UV photoproducts are first recognized by UV-DDB (18, 21, 22). Stable binding of UV-DDB to sites of damage activates the ubiquitination activity of $CRL4^{DDB2}$, which targets histones, primarily H2A, and enables nucleosome disassembly and subsequent recruitment of the XPC complex, which is also a ubiquitination substrate (18–24). Lesion handover between $CRL4^{DDB2}$ and XPC is thought to be achieved by the autoubiquitination of DDB2 at lysines in the intrinsically disordered N terminus of DDB2 (18, 21). This modification of DDB2 serves to flag the repair factor for degradation (25).

We recently provided crystallographic and biophysical evidence for the dimerization of UV-DDB at sites of damage (26). The identification of this dimeric UV-DDB complex on DNA reveals a previously unanticipated complexity in damage recognition and raises several important questions in the initial damage recognition step of human GG-NER. In this study, we sought to answer: How do ∼180,000 molecules of UV-DDB (14) scan 3.2 billion bp of genomic DNA to find relatively rare lesions in DNA? How does UV-DDB interrogate the DNA to achieve remarkable specificity in damage discrimination? How does dimeric UV-DDB modulate the specificity of damage discrimination? How do mutations in the DNA-binding interface found in the K244E mutant of DDB2 influence the kinetics of DNA binding and damage recognition?

To better understand damage recognition by UV-DDB, we used a single-molecule DNA tightrope assay (27–30) to observe the real time interactions of quantum dot (QD)-conjugated wild-type (WT) UV-DDB or UV-DDB containing the K244E mutation in DDB2, with damaged DNA substrates with high temporal and spatial resolution. Observations of individual molecules reveal the presence of short-lived intermediates and heterogeneity in molecular properties that may be lost due to bulk averaging of the properties of an unsynchronized ensemble of molecules. We found that WT UV-DDB performs a 3D search to locate UV damage in DNA, whereas UV-DDB containing the K244E mutation in DDB2 slides on DNA. Unexpectedly, we identified multiple kinetic intermediates that participate in a complex kinetic cascade of damage recognition by WT UV-DDB. Here, we propose a working model wherein UV-DDB conformationally proofreads (31) DNA and uses dimerization as a strategy to enhance specificity of the damage recognition process.

Results

Visualizing the DNA Damage Search Mechanism of UV-DDB. UV-DDB could use a number of different approaches to find DNA damage (*SI Materials and Methods*, section 1.1 and Fig. S1*A*), as reviewed in ref. 32, and single-molecule methods have been used to experimentally validate and visualize various protein search strategies (27, 28, 33–35). We have previously developed a DNA tightrope assay that enables the direct visualization of dynamics of QD-conjugated proteins on DNA (27–30). Briefly, in this assay, λ-DNA tightropes are strung-up between 5-μm poly-L-lysine–coated beads, which are deposited on a PEGylated coverslip (Fig. 1 *A* and *B*). Biomolecular interactions on DNA tightropes in the absence of buffer flow and surface interactions are visualized by oblique-angle fluorescence microscopy imaging (Fig. 1*A*). A schematic of the flow cell under oblique-angle illumination is shown in Fig. 1*A* and a YOYO-1–stained image of DNA obtained using oblique-angle fluorescence microscopy is shown in Fig. 1*C*.

QD UV-DDB Performs a 3D Search on Undamaged as Well as UV-Damaged DNA. To observe the interactions of UV-DDB with DNA, we conjugated UV-DDB to streptavidin-coated QDs (SA-QDs). These nanoparticles provide superior brightness and resistance to photobleaching compared with conventional fluorophores and fluorescent proteins (36, 37). To that end, we systematically tested three strategies for conjugating QDs to UV-DDB and proceeded with a His-Ab conjugation strategy that enabled us to conjugate UV-DDB to SA-QDs using a biotinylated penta-His antibody, while retaining DNA damage binding activity (*SI Materials and Methods*, section 1.2.3) (29). We incubated QD UV-DDB with undamaged λ-DNA tightropes or λ-DNA containing on average one lesion per 2,200 bp (*SI Materials and Methods*, section 2) and observed these interactions in a time window of 900 s. Imaging was performed in the absence of YOYO-1 dye to minimize potential double-strand breaks in the DNA tightropes (*SI Materials and Methods*, section 1.2.4) (38). We observed the binding of UV-DDB to DNA (Fig. 1*D*; undamaged DNA, Movie S1; UV-damaged DNA, Movie S2). For both undamaged and

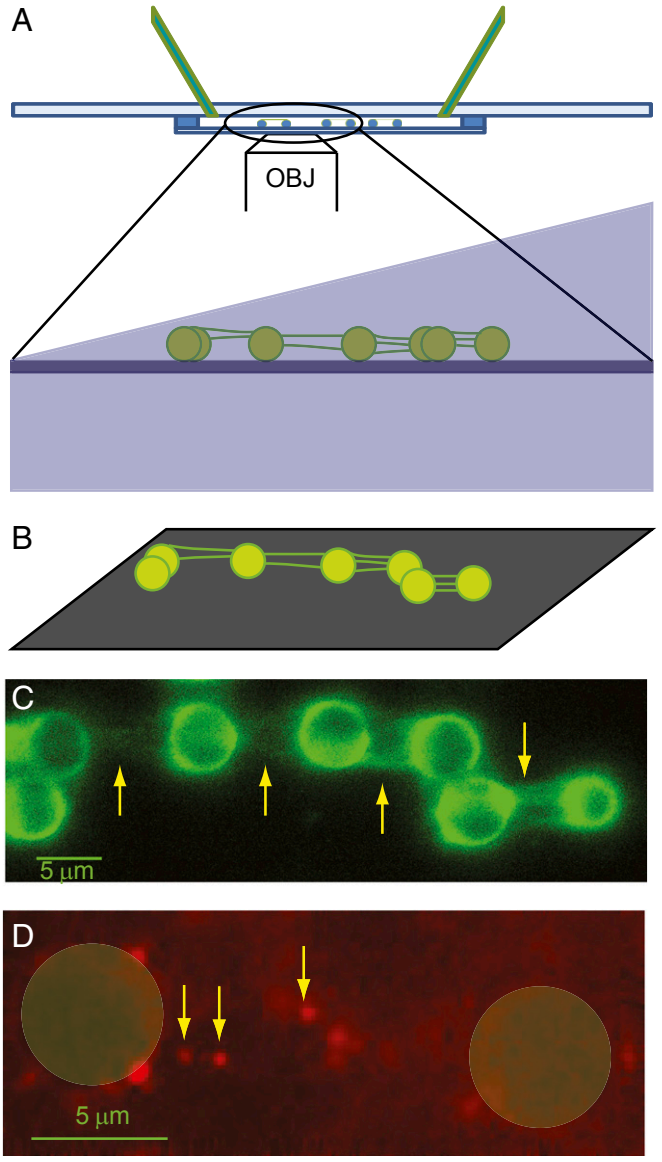

Fig. 1. (*A*) Schematic of flow cell and microscope setup used in the DNA tightrope assay with oblique-angle illumination. (*B*) Schematic of 5-μm poly-L-lysine–coated beads deposited on a PEGylated glass surface with DNA tightropes elongated between them. (*C*) Oblique-angle fluorescence microscopy image of YOYO-1–stained λ-DNA tightropes (arrows) between poly-L-lysine–coated beads. Arrows indicate DNA between beads. (*D*) Image of QD UV-DDB binding to unstained DNA tightropes between beads (shown by green masks). Arrows indicate bound QD UV-DDB (Fig. S1 and Movie S1).

UV-damaged DNA, four classes of binding events were identified in a typical 900-s observation window (Fig. 2 *A–D*). These included molecules that (*i*) are present at the start of observation, but dissociate during observation ("dissociate" in Fig. 2*A*); (*ii*) associate during observation and are present at the end of observation ("associate" in Fig. 2*B*); (*iii*) are present both at the start and end of observation ("persistent" in Fig. 2*C*); and (*iv*) both associated and dissociated during observation ("transient" in Fig. 2*D*). In the majority of cases (>98%, n = 990 events), upon incubation with either undamaged or UV-damaged DNA, QD UV-DDB molecules associated with the DNA and did not show any sliding behavior (Movies S1 and S2) within the limits of our spatial and temporal resolutions (36 nm, ~100 bp, 100 ms; *SI Materials and Methods*, section 1.3). Taken together, these data indicate that UV-DDB probes for DNA damage using a 3D search mechanism. Because these assays were performed in the absence of flow, we were able to observe macroscopic dissociation and rapid reassociation behavior of UV-DDB on separate DNA molecules, a phenomenon that is consistent with "jumping" (Fig. S2*B* and Movie S1), which we have reported previously for bacterial UvrA (28).

UV Radiation-Induced DNA Photoproducts Shift the Binding Equilibrium to Longer-Lived States. The presence of UV-induced photoproducts at a density of about one lesion per 2.2 kb of λ-DNA alters and greatly increases the binding of UV-DDB molecules (Fig. 2*E*, n = 347 for nondamaged DNA and n = 643 for damaged DNA). For example, UV damage caused a 2.5-fold increase in the molecules that persisted for all 900 s of observation time (Fig. 2 *E* and *F*). Furthermore, UV-induced damage caused an eightfold increase in UV-DDB molecules that associated onto the DNA during this 900-s observation window (Fig. 2 *E* and *F*). As expected, DNA damage decreases the percentage of transient UV-DDB molecules (Fig. 2*D*, those that bound and then dissociated) on UV-irradiated λ-DNA molecules (compare 67.8% vs. 88.8% for nondamaged DNA which was not UV irradiated, respectively, Fig. 2 *E* and *F*). These data reveal that across all these classes of binding events, UV-DDB associates with and persists on DNA for longer time periods when the DNA tightropes contain UV damage while showing lower transient behavior.

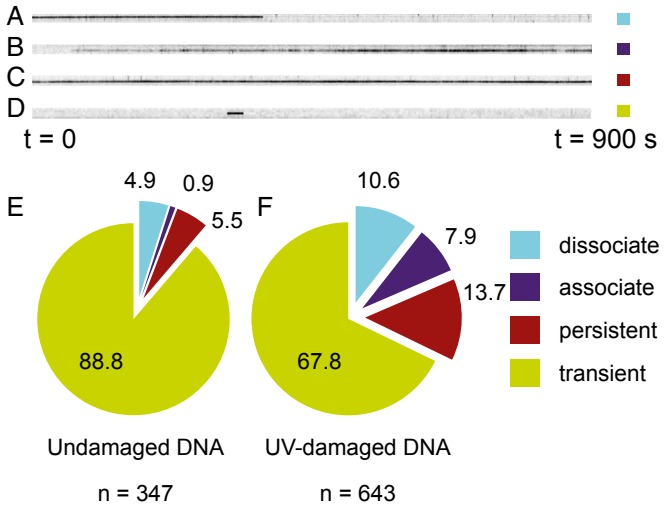

Fig. 2. Kymographs of individual QD UV-DDB molecules that (*A*) dissociate from DNA during observation, (*B*) associate with DNA during observation, (*C*) are present during the entire observation window, and (*D*) both associates and dissociates during observation (transients). (*E* and *F*) Pie chart of percentage of each of the observations described above for undamaged DNA (n = 347) and UV-damaged DNA (n = 643), respectively (Fig. S2 and Movies S1 and S2).

Single-Molecule Visualization Reveals Multiple Kinetic Intermediates of UV-DDB. To further understand the heterogeneity in dwell times and to extract rate constants, we analyzed the kinetics of transient binding on both undamaged and UV-damaged DNA. Dissociation of UV-DDB complexes on DNA can be modeled as a first-order decay (Poisson) process from the DNA-bound intermediate state to the DNA-free state (*SI Materials and Methods*, section 3.1.1). With the objective of quantifying this process, we performed a cumulative residence time distribution (CRTD) analysis (*SI Materials and Methods*, section 3.1.2) (39). The CRTD may be interpreted as a type of survival curve representing the fraction of the population of DNA-bound proteins remaining on DNA as a function of time. Fitting the CRTD to a Poisson process ($T \equiv \exp\{-k_d t\}$) yields the dissociation rate constant (k_d) and consequently the mean lifetime ($\tau = k_d^{-1}$) of particles dissociating from the DNA. For systems comprised of multiple intermediates, the number of terms fit to the CRTD reveals the number of measurable intermediates (*SI Materials and Methods*, section 3.1.2 and Table S1).

The CRTDs describing the data for transient binding (Fig. 2*D*) to undamaged DNA and damaged DNA are presented in Fig. 3 *A* and *B*, respectively. Binding events that persisted for the entire 900-s observation window were necessarily excluded from this analysis. Examination of these CRTDs on undamaged DNA revealed the presence of three kinetic intermediates with mean lifetimes over three orders of magnitude (0.8, 8.1, and 113 s; Table 1). Surprisingly, we detected similar kinetics for transiently bound UV-DDB on UV-damaged DNA. However, as described below, we found that UV damage enriched the population of the longest-lived intermediates on DNA indicating that more UV-DDB bound with higher affinity on DNA containing UV damage. We found that all of the features of each of the CRTDs were best described when three exponentials terms corresponding to three decay processes were used (*SI Materials and Methods*, sections 3.1.1, 3.1.2, and 3.2; log-log representation Fig. S3 *A* and *B*; log-linear representation Fig. S3 *C* and *D*). We denote these three independent Poisson processes that describe the dissociation kinetics of transiently bound UV-DDB as $T_{1,ud}$, $T_{2,ud}$, and $T_{3,ud}$ (Table 1 and *SI Materials and Methods*, sections 3.1.1, 3.1.2, and 3.2). Analysis of the dwell times, τ, of UV-DDB on UV-damaged DNA also revealed three kinetic intermediates which dissociate from DNA according to three Poisson processes: $T_{1,d}$, $T_{2,d}$, and $T_{3,d}$ (Table 1 and *SI Materials and Methods*, sections 3.1.1, 3.1.2, and 3.2). It is important to note that the detection of decay processes in the CRTD analysis of transient molecules is limited by the time resolution, size of the time window of acquisition, and the probability of occurrence of the decay process. Given that the time resolution of acquisition (0.1 s) is of the order of the mean lifetime of UV-DDB molecules dissociating according to the T_1 process (0.3s, 0.8s), the apparent differences between $T_{1,ud}$ and $T_{1,d}$ processes may be biologically indistinguishable. It is noteworthy that the T_1 process identified here does not correspond to nonproductive collisions that are found to occur on an ~100× faster time scale (~5 ms) (35).

To better understand how the presence of photoproducts in the DNA changes the extent of UV-DDB binding, we first calculated the fraction of the population dissociating from each DNA substrate according to the decay processes identified above (Table 1). We then compared the relative fractions of the three kinetic intermediates represented on each DNA substrate (Fig. 3 *C* and *D* and *SI Materials and Methods*, section 3.3). In the population of molecules bound to undamaged DNA, 58% were found to dissociate with a lifetime of $\tau_{1,ud}$ (0.8 s) compared with 57% for UV-damaged DNA with a lifetime of $\tau_{1,d}$ (0.3 s). Similarly, 35% were found to dissociate from undamaged DNA

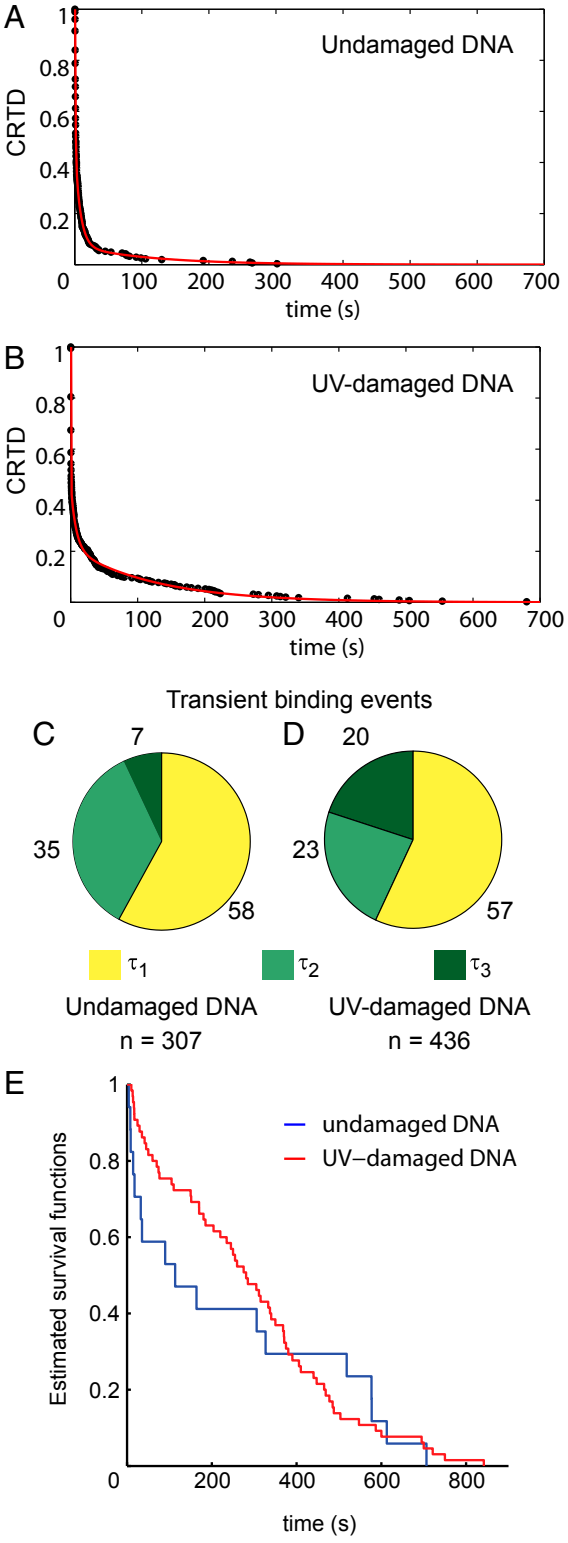

Fig. 3. CRTD plots for transient UV-DDB (Fig. 2*D*) dissociating from (*A*) undamaged DNA and (*B*) UV-damaged DNA with experimental data in black circles and triple exponential fits (red). (*C* and *D*) Pie chart showing the percentage of molecules participating in each of the three Poisson processes (Table 1) observed in the transient binding events (Fig. 2*D*) observed for binding to undamaged DNA (n = 307) or UV-damaged DNA (n = 436), respectively. (*E*) Estimated survival functions for dissociating molecules (Fig. 2*A*) from undamaged DNA (blue, n = 16) and UV-damaged DNA (red, n = 67) (Fig. S3 and Table 2).

compared with 23% for UV-damaged DNA (1.5-fold higher) with a lifetime of τ_2 (8 s) and 7% of the molecules dissociated with a lifetime of τ_3 (120 s) compared with 20% for binding to UV-damaged DNA (2.9-fold higher; Fig. 3 *C* and *D*). These data indicate that a greater fraction of UV-DDB dissociates according to the T_2 process on undamaged DNA compared with that on UV-damaged DNA. This suggests that the T_2 process is a damage verification process which facilitates the dissociation of weakly bound UV-DDB molecules on DNA.

These data also indicate that the fraction of molecules that do not dissociate according to the T_2 process, participate in a much slower, T_3 process. We found that a 2.9-fold greater fraction of UV-DDB dissociates, according to the T_3 process, from UV-damaged DNA compared with undamaged DNA. These results indicate that the T_3 process represents the slow dissociation of a tightly bound kinetic intermediate of UV-DDB, which is represented to a greater extent on UV-damaged DNA.

Further evidence for the presence of long-lived complexes was the class of observations that are present at the beginning of data acquisition and dissociate during observation (Fig. 2*A*). We performed a CRTD analysis for this class of particles and obtained the survival curves presented in Fig. 3*E* for undamaged DNA (n = 16, blue) and damaged DNA (n = 67, red). We found that this population dissociated from undamaged λ-DNA according to the T_2 process ($\tau_{2,ud}$ = 11.7 s) and a distinct T_4 process ($\tau_{4,ud}$ = 446.2 s; Table 2 and *SI Materials and Methods*, section 3.5). Additionally, we found that UV-DDB also dissociated from UV-damaged λ-DNA according to a T_4 process with $\tau_{4,d}$ = 336.7 s (Table 2 and *SI Materials and Methods*, section 3.5).

WT UV-DDB Is Persistent on UV-Damaged DNA and Slides at High Ionic Strength. As mentioned above, we detected a population of molecules that persisted during the entire observation window of 900 s (Fig. 2*C* and Movie S2), with some individual molecules persisting for up to 90 min. Importantly, these persistent molecules represent a distinct, stable complex that does not dissociate according to any of the T_1, T_2, T_3, or T_4 processes described here (*SI Materials and Methods*, section 4.1). UV damage caused a 2.5-fold increase in these persistent UV-DDB molecules. Furthermore, these persistent molecules exhibited a salt-dependent mobility and are not irreversible aggregates of UV-DDB on DNA (*SI Materials and Methods*, section 4.2, Fig. S4, and Movie S3).

UV-DDB Colocalizes and Is Persistent at Sites of Lesions. We posited that long-lived UV-DDB molecules on UV-damaged λ-DNA represented UV-DDB bound to sites of photoproducts. Because UV-DDB has previously been demonstrated to bind DNA containing an abasic site (AP site) analog with high affinity (14), we engineered long DNA substrates containing defined AP sites every 2 kb, for use in the DNA tightrope assay (*SI Materials and Methods*, section 5.1) (40). To identify the site of the lesion in these long DNA substrates, we engineered a biotin modification near the AP site. This enabled us to mark the site of the lesion using SA-QDs and test the hypothesis that UV-DDB is long-lived at sites of lesions in these DNA damage arrays. Upon incubation with SA-QDs, we were able to observe QD arrays on these substrates marking sites of introduced biotins in the proximity of the AP sites (APbiodT) (Fig. 4*A*). The pair-wise inter-QD distances were consistent with integral multiples of the linearized plasmid length of 0.65 μm (Fig. 4*B*). This distribution reflects the probability of occurrence of pairs of QDs with discrete numbers of plasmid lengths between them. This skewed distribution arises from the distribution of DNA substrate lengths, as well as the lower number of pairs of QDs with large number of plasmid lengths between them on any given DNA molecule. To investigate whether long-lived UV-DDB molecules bound DNA at sites of DNA damage, we performed dual-color experiments

Table 1. Estimates for the amplitudes and dissociation rate constants for transient molecules

		Analysis of transient molecules								
		T_1			T_2			T_3		
DNA type	N	a_1	$k_{d,1}$, s^{-1}	τ_1, s	a_2	$k_{d,2}$, s^{-1}	τ_2, s	a_3	$k_{d,3}$, s^{-1}	τ_3, s
Undamaged DNA	307	0.79	1.22	0.8	0.39	1.23×10^{-1}	8.1	0.07	8.85×10^{-3}	113.0
Lower bound of 95% CI		0.76	1.13	0.8	0.37	1.07×10^{-1}	7.2	0.05	4.50×10^{-3}	75.8
Upper bound of 95% CI		0.81	1.31	0.9	0.41	1.40×10^{-1}	9.3	0.09	1.32×10^{-2}	222.1
Damaged DNA	436	1.11	3.03	0.3	0.25	1.25×10^{-1}	8.0	0.21	7.89×10^{-3}	126.7
Lower bound of 95% CI		1.03	2.78	0.3	0.24	1.09×10^{-1}	7.1	0.20	7.13×10^{-3}	115.4
Upper bound of 95% CI		1.19	3.28	0.4	0.27	1.41×10^{-1}	9.2	0.22	8.66×10^{-3}	140.4

N represents the total number of observed counts. a_i represent the coefficient of the exponential terms obtained from the fits. $k_{d,i}$ represent the dissociation rate constants and τ_i represent the mean lifetimes. The lower and upper bounds corresponding to the 95% confidence intervals (CI) are presented for the population of transient molecules observed in this study.

involving the incubation of QD UV-DDB conjugates with QD-conjugated APbiodT DNA tightropes. We found long-lived UV-DDB molecules that colocalized to sites of damage (n = 22; Fig. 4*C*, Movie S4, and *SI Materials and Methods*, section 5.2) and persisted through the entire observation window. Significantly, this general method of creating long DNA substrates with site-specific modifications provides new opportunities for studying site-specific interactions of DNA repair proteins in the DNA tightrope platform.

Dimeric UV-DDB Is Persistent at Sites of Damage. Previously we identified that UV-DDB dimerizes on DNA (26). We next probed whether the long-lived intermediates detected in this study represented dimeric UV-DDB. To address the nature of UV-DDB stoichiometry, we incubated UV-DDB molecules which had been separately labeled with two differently colored QDs, together with UV-damaged DNA tightropes. We observed colocalization of both colors representing dimerization of WT UV-DDB (Movie S5 and Fig. 4*D*). This colocalization did not exhibit a dependence on the choice of QD conjugate. In addition, we found that 13 (72%) of 18 observations of dual-colored dimeric UV-DDB complexes (compared with a total of 47 single-colored persistent UV-DDB) persisted during the entire observation window of 900 s, indicating that UV-DDB dimers are long-lived on UV-damaged DNA. Additionally, long-lived UV-DDB dimers were also observed on APbiodT substrates (n = 18 dual-colored complexes and n = 67 single-colored persistent UV-DDB; Fig. 4*E*). Control EMSA experiments revealed that UV-DDB binds to biodT containing substrates essentially the same as undamaged DNA substrates (*SI Materials and Methods*, section 5.3 and Fig. S5*C*), confirming that the colocalization observed in these experiments indeed reflects dimeric UV-DDB at abasic sites in the DNA.

UV-DDB Containing the K244E Mutant of DDB2 Dimerizes and Slides on DNA. To gain insight into the structural nature of the complex binding kinetics of WT UV-DDB, we turned our attention to an XP-causing mutant of UV-DDB containing the K244E mutation in DDB2 [UV-DDB (K244E)] found in the XP82TO patient. This UV-DDB (K244E) variant contains a mutation in a crucial DNA-binding residue in DDB2, which greatly reduces its affinity for DNA and its specificity for damage (14, 24). We probed the DNA-binding ability of recombinant UV-DDB (K244E) in a pull-down experiment (see *SI Materials and Methods*, section 6.1 for details) and found that, consistent with a previous report (24), UV-DDB (K244E) lacks the ability to discriminate UV-induced damage in DNA while retaining strong end binding (*SI Materials and Methods*, section 6.1 and Fig. S6*A*). This finding was further confirmed by atomic force microscopy (AFM) experiments in which UV-DDB (K244E) was incubated with undamaged DNA (Fig. 5 *A* and *B* and *SI Materials and Methods*, section 6.2). UV-DDB (K244E) possesses residual DNA-binding activity mostly at DNA ends, exhibiting a threefold preference for binding to two DNA molecules over a single DNA molecule (*SI Materials and Methods*, section 6.2).

To obtain dynamic information describing the binding of UV-DDB (K244E) to DNA, we incubated QD UV-DDB (K244E) with undamaged λ-DNA in the DNA tightrope assay. We found that overall binding of UV-DDB (K244E) was diminished and in stark contrast to the WT UV-DDB, 80% (79 of 99 observations) of UV-DDB (K244E) molecules exhibited sliding behavior. Next we wanted to identify whether UV-DDB (K244E) was able to

Table 2. Estimates for the amplitudes and dissociation rate constants for dissociating molecules

		Analysis of dissociating molecules							
		T_4				T_2			
DNA type	N	a_4	$k_{d,4}$, s^{-1}	τ_4, s	N	a_2	$k_{d,2}$, s^{-1}	τ_2, s
Undamaged DNA	11	0.71	2.24×10^{-3}	446.2	5	0.42	0.85	11.7
Lower bound of 95% CI		0.62	1.78×10^{-3}	370		0.28	0.01	6.5
Upper bound of 95% CI		0.79	2.70×10^{-3}	562.1		0.60	0.15	63.3
Damaged DNA	67	1.02	2.97×10^{-3}	336.7				
Lower bound of 95% CI		0.99	2.79×10^{-3}	317.5				
Upper bound of 95% CI		1.06	3.15×10^{-3}	358.6				

N represents the total number of observed counts. a_i represent the coefficient of the exponential terms obtained from the fits. $k_{d,i}$ represent the dissociation rate constants and τ_i represent the mean lifetimes. The lower and upper bounds corresponding to the 95% CIs are presented for the population of dissociating molecules observed in this study.

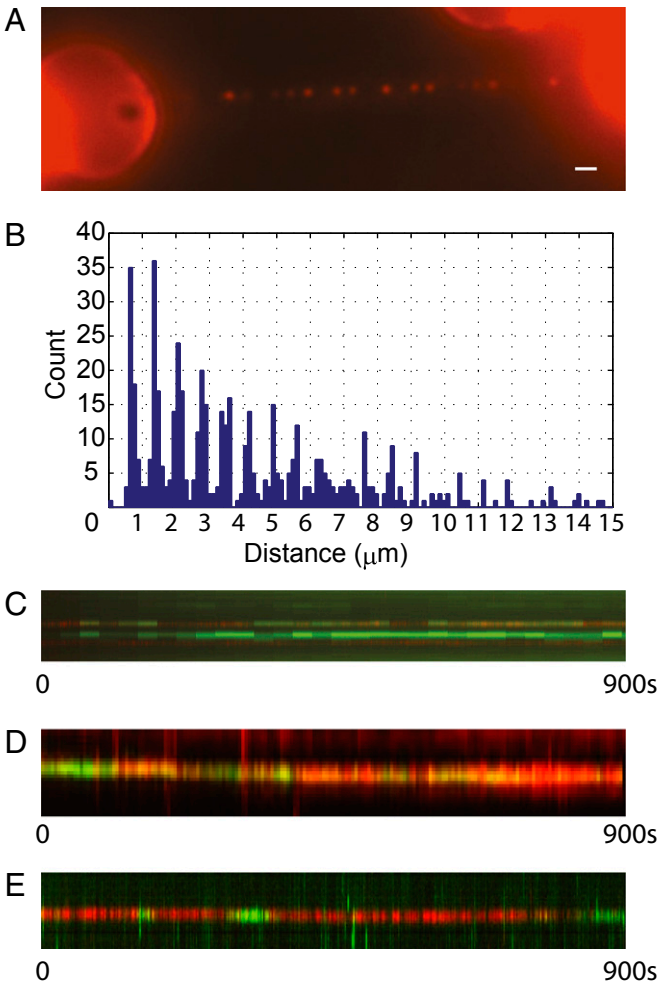

Fig. 4. (*A*) Oblique-angle fluorescence microscope image of array of QDs on a DNA tightrope of a long DNA molecule containing a defined abasic site analog with a proximal biotin marking the site of the lesion. (Scale bar: 1 μm.) (*B*) Histogram of pairwise distances between QDs marking sites of the introduced lesion. (*C*) Kymograph of UV-DDB (red) colocalized to sites of defined lesion (green) (one pixel = 46 nm along *y* axis) (Movie S4). Here, data in the red channel was collected at 10 fps whereas data in the green channel was collected at 0.3 fps. (*D* and *E*) Dual-color kymographs of the UV-DDB dimer on UV-damaged DNA (Movie S5) and APbiodT substrate, respectively (one pixel = 46 nm along the *y* axis) (Fig. S5 and Movies S4 and S5).

stably colocalize to sites of damage. We incubated the mutant protein with DNA tightropes containing defined abasic site analog lesions (APbiodT) and found that UV-DDB (K244E) was also found to slide on APbiodT DNA without exhibiting obvious long-lived pausing behavior (Movie S6 and Fig. 5*C*). This finding is consistent with the findings from the pull-down experiment which indicate that UV-DDB (K244E) lacks the ability to stably associate with DNA damage (Fig. S6*A*). Of the sliding UV-DDB (K244E) molecules, we calculated diffusion constants for molecules that were found to slide on DNA for an observation window of at least 60 s. Sliding QD UV-DDB (K244E) exhibited heterogeneity in its diffusive behavior spanning three orders of magnitude (Fig. 5*D* and *SI Materials and Methods*, section 6.3). Importantly, the diffusive behavior of UV-DDB (K244E) on DNA (both undamaged λ-DNA and APbiodT) was found to have a mean diffusion constant of 0.11 ± 0.2 $\mu m^2 \cdot s^{-1}$ (mean ± SD), with an anomalous diffusive exponent (α) of 0.5 ± 0.22 (mean ± SD) (n = 31, *SI Materials and Methods*, section 6.3).

Unexpectedly, the DNA tightrope assay provided further insight into the interaction of UV-DDB (K244E) with DNA. We identified rare events that suggest that dimerization of UV-DDB (K244E) is DNA dependent and proceeds via random collisions of UV-DDB (K244E) molecules on DNA (Movie S7 and Fig. S6*C*). This observation prompted us to examine the stoichiometry of UV-DDB (K244E) bound to DNA. We have previously used AFM to identify the stoichiometry of WT UV-DDB bound to DNA using a calibration curve relating the AFM volume of the complex to its molecular weight (*SI Materials and Methods*, section 6.5 and Fig. S6*D*) (26). Volume analysis of DNA-bound UV-DDB (K244E) revealed a peak at 564.3 ± 10.1 nm^3 corresponding to a molecular weight of 388.6 ± 11.8 kDa (mean ±

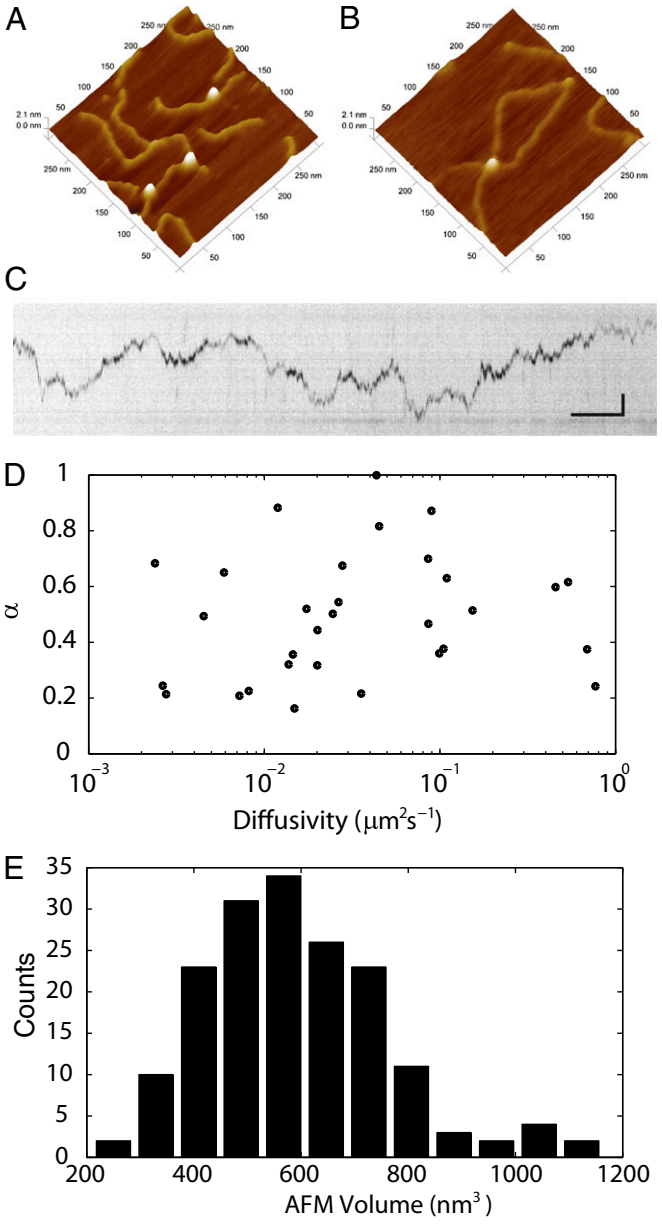

Fig. 5. AFM images of UV-DDB (K244E) bound to (*A*) 517-bp DNA, or (*B*) plasmid DNA demonstrating that UV-DDB (K244E) dimerizes on DNA, 300 nm × 300 nm × 2 nm. (*C*) Kymograph of K244E sliding on DNA. (Vertical scale bar: 1 μm; horizontal scale bar: 5 s.) (*D*) Plot of anomalous diffusive exponent vs. diffusivity for sliding UV-DDB (K244E) (Movie S6). (*E*) Histogram of UV-DDB (K244E) volumes on DNA (n = 171) (Fig. S6 and Movie S6).

SD), consistent with that of dimeric UV-DDB (K244E) bound to DNA ($n = 171$, Fig. 5*E*). These data demonstrate that a mutation in the DNA-binding interface of DDB2 does not inhibit dimerization of UV-DDB. However, in contrast to WT UV-DDB (26), dimeric UV-DDB (K244E) is more likely to be stabilized on two DNA molecules in a damage-independent manner (*SI Materials and Methods*, section 6.2). In summary, our study indicates that UV-DDB (K244E) retains the ability to dimerize on DNA but lacks specificity for lesions and consequently slides on DNA.

Discussion

In this study, we used single-molecule techniques to understand the kinetics of damage recognition by UV-DDB in the initial step of NER. We identified that UV-DDB consisting of DDB1 and DDB2 performs a 3D search for damage sites in DNA. Using DNA substrates containing UV-induced photoproducts or AP sites, we discovered a complex kinetic pathway of damage recognition by UV-DDB that culminates in the formation of long-lived dimers of UV-DDB [$(DDB1\text{-}DDB2)_2$] at sites of damage. Specifically, we found that UV photoproducts or abasic sites (*i*) increased the total number of stably bound UV-DDB molecules, (*ii*) decreased the number of transient UV-DDB molecules that associate and dissociate from DNA, (*iii*) increased the number of UV-DDB molecules that associate and persist on DNA, and (*iv*) substantially increased the number of persistent dimers of UV-DDB on DNA. Additionally, we studied the stoichiometry and dynamics of the XP causing K244E mutant of DDB2 on DNA and identified that UV-DDB (K244E) dimerizes and slides on DNA but does not stably associate to damaged sites.

Damage Recognition Is a Multistep Kinetic Cascade Culminating in UV-DDB Dimerization. The use of our single-molecule tightrope platform permitted the observation of previously undetected kinetic intermediates in the process of damage recognition by UV-DDB. We found evidence for five, progressively stable kinetic intermediates, four of which were transient and the fifth was found to be persistent during the 900-s observation window (*SI Materials and Methods*, section 3.4). Some of the slower decay processes detected here are consistent with previously available bulk estimates (*SI Materials and Methods*, section 7) and likely represent dissociation of bound UV-DDB from lesions in DNA (15, 17, 26). Likewise, some of the long-lived intermediates on undamaged DNA probably represent UV-DDB bound to spontaneous damage arising from depurination on commercially available λ-DNA, which is recognized by UV-DDB (14).

Dual-color fluorescence microscopy experiments revealed that dimeric UV-DDB persists on damaged DNA tightropes. Previous AFM experiments revealed that four of five WT UV-DDB complexes on DNA consisted of dimeric WT UV-DDB bound to a single DNA molecule (26). In contrast, 76% of dimeric UV-DDB (K244E) complexes on DNA were bound to two molecules of DNA (Fig. 5 *A* and *B* and *SI Materials and Methods*, section 6.2). These findings indicate that the presence of two DNA molecules in the dimeric UV-DDB DNA complex is a sufficient but not necessary requirement for dimerization.

We predict that these long-lived dimers of UV-DDB at sites of lesions could inhibit the progression of NER if these highly stable UV-DDB dimers are not actively dismantled. In support of this hypothesis, introduction of excess recombinant UV-DDB to in vitro reconstituted NER reactions resulted in inhibition of repair of (6–4) photoproducts (8, 9). In addition, in vivo studies of fluorescently tagged UV-DDB binding have reported immobile binding of UV-DDB to DNA for up to 4 h in XP-A cells (41). In a study involving siRNA knockdown of Cullin4A, fluorescently tagged UV-DDB exhibited delayed disappearance from CPD foci in HeLa cells (42). Inhibition of the proteasome using MG132 also resulted in inhibited recruitment of XPC to sites of CPD lesions in mammalian cells (43). We believe that the highly stable, persistent, dimeric UV-DDB complexes detected in our studies represent a distinct species on the kinetic pathway to recognize damage with high specificity and affinity.

Damage Recognition Involves Dynamic Conformational Changes in both UV-DDB and DNA. What might be the physical basis of the heterogeneity observed in the lifetimes of the repair intermediates? Crystal structures of UV-DDB in the apo and DNA damage-bound forms give insight into this question [Protein Data Bank (PDB) ID codes 3EI1 (44), 4A0A, 4A0K, (18) and 4E54 (26)]. The protein in the apo state [PDB ID code 3EI4 (18)] upon binding to damaged DNA undergoes an FQH hairpin (F334-Q335-H336) transition which probes the major groove of the DNA for the presence of damage [PDB ID code 4E45 (26); Fig. 6 *A* and *D* and Movie S8] (18, 26, 45). At sites of damage, this conformational change in DDB2 is accompanied by the base flipping of the damaged bases in DNA (consisting of the photoproducts in the case of UV damage, alternatively the abasic site and the adjacent 3′ base; Fig. 6 *B* and *D*) to an extrahelical conformation and stabilization in the lesion binding pocket of DDB2 (PDB ID codes 3EI1, 4A0A, and 4A0K) (18, 44). Stable damage recognition is thought to induce folding of the intrinsically disordered N terminus to form an α-paddle structure, which along with the β-wing, forms a winged helix structure upon DNA binding (PDB ID code 4E54; Fig. 6*D*) (18, 26). Damage recognition may thus be considered to progress along a reaction coordinate that describes a series of dynamically interconverting structural intermediates. Some of the highly transient, short-lived binding intermediates observed in this work might reflect abortive attempts at damage recognition by UV-DDB. These species may correspond to metastable intermediates that participate in varying extents of lesion engagement, failing to stabilize at sites of lesions. Indeed, previous work has demonstrated that the assembly and disassembly of subunits of large macromolecular complexes such as the spliceosome proceeds via a kinetic pathway, which rejects nonproductive subcomplexes along the reaction coordinate (46).

K244 Is Required for Damage Recognition. Specific damage recognition depends on K244 switching its conformation in the apo form to the DNA-bound form (Fig. 6*A*). We have demonstrated that the DDB2 K244E mutant supports UV-DDB dimerization but slides on DNA and fails to stably engage lesions. This finding suggests that processing of damaged DNA is contingent upon the successful sandwiching of the undamaged base 3′ to the two damaged bases, between the FQH hairpin and K244. The dimerization of UV-DDB (K244E) observed in our AFM experiments probably occurs by rapid 3D diffusion of one UV-DDB (K244E) molecule colliding with another, the DNA-bound UV-DDB (K244E) (Movie S7). Such a dimer may form a topologically constrained complex on the DNA, which is not actively engaged in a damage detection conformation (Fig. 6*E*). The subdiffusive nature of the UV-DDB (K244E) sliding indicates that this complex performs a constrained Brownian walk on the DNA, suggesting that although mutant DDB2 cannot bind to DNA damage to form persistent complexes, it has several strong interactions with the DNA, such as helix probing with the FQH motif (29). This sliding state may arise from either a conformational change in the monomer of UV-DDB (K244E) that is capable of sliding, or from dimeric UV-DDB (K244E) that fails to stably engage the lesion.

Conformational Proofreading Is a Candidate Mechanism for Damage Recognition. As evidenced from the crystal structures, both UV-DDB and the DNA undergo a series of concerted conformational changes that ensure successful damage recognition [PDB ID codes 3EI4 (45), 3EI1 (18), 4A0A, 4A0K (18), and 4E54

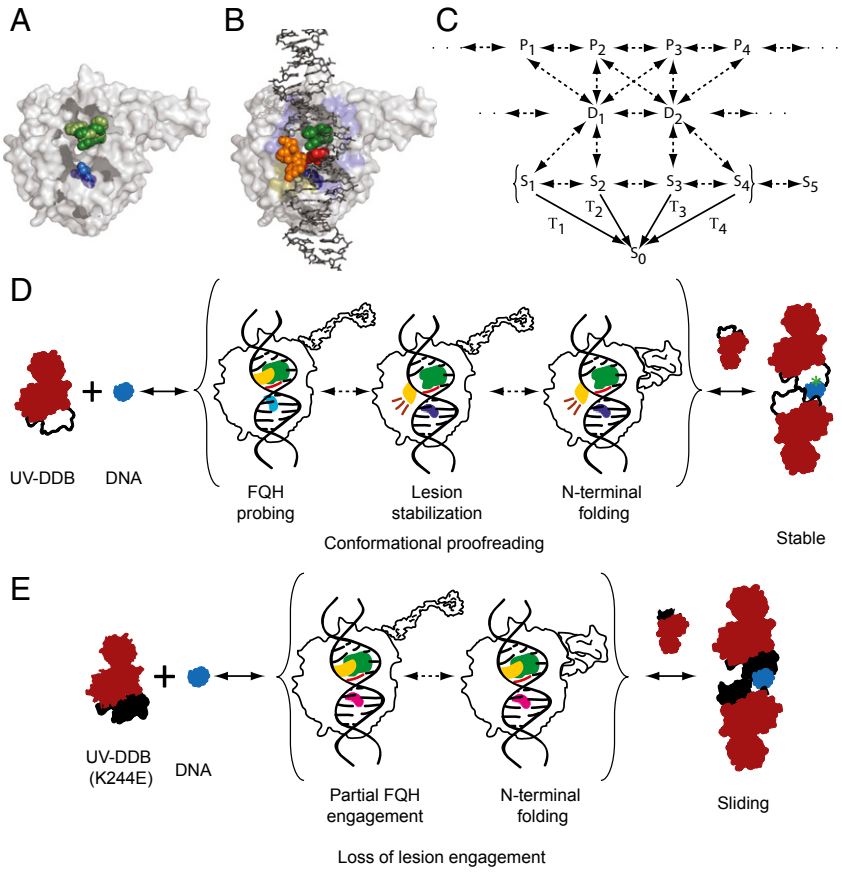

Fig. 6. (*A*) Molecular model of DDB2 showing conformations of the FQH motif (green) and K244 (blue) in the apo (light) and DNA-bound (dark) states [PDB ID codes 3EI4 (45) and 4E54 (26)]. (*B*) DNA-binding interface of DDB2 illustrating the pinning of the undamaged base adjacent (red) to the lesion (orange) between the FQH motif (green) and K244 (dark blue) (PDB ID code 4E54). The molecular recognition scheme presented in *C* shows a small, illustrative subset of interconverting protein {P} and DNA {D} conformers which form intermediates {S}, whose decay rates are measured in this work (species in brackets). (*D*) Model for damage recognition and conformational proofreading by WT UV-DDB where green represents the FQH hairpin, blue represents K244, and yellow represents the lesion. This model highlights some of the known conformations of UV-DDB in the apo state and bound to DNA damage. (*E*) Model for sliding behavior of K244 on DNA, where magenta represents the glutamate in K244E DDB2 and other colors as described above (Movie S8).

(26)]. This problem of damage recognition by UV-DDB falls under a category of problems in molecular recognition which use conformational changes in the target and/or the ligand to achieve highly specific recognition in a noisy environment. This mechanism termed "conformational proofreading" (31) uses a structural mismatch between the protein-binding pocket and the ligand such that binding of the correct ligand facilitates a conformational change in the protein which stabilizes the binding, whereas the incorrect ligand is unlikely to allow this conformation change and is therefore rejected. This mechanism of conformational proofreading describes specific molecular recognition in the absence of energy consumption and is an alternative to kinetic proofreading (31, 47).

A working model for damage recognition by WT UV-DDB is presented here (Fig. 6 *C* and *D* and *SI Materials and Methods*, section 3.4). Each of the intermediate states detected here, $\{S_i\}$, can be considered to be comprised of a protein configuration $\{P_i\}$ and a DNA configuration $\{D_i\}$ (*SI Materials and Methods*, section 3.4). Here, the apo protein and the DNA interconvert between ensembles of conformers $\{P_i\}$ and $\{D_i\}$. Collisions between the protein and DNA result in the formation of interconvertible repair intermediates $\{S_i\}$, some of which are relatively stable and observable (such that their decay to the DNA-free state $\{S_0\}$ is measurable). We propose that during the initial stages of damage recognition by WT UV-DDB, target specificity arises from the ability of the repair intermediate to cross energy barriers between the various states, whereas additional affinity arises from the dimerization of WT UV-DDB, which then locks the repair factor to the site of damage. The formation of dimers of mutant UV-DDB (K244E) on DNA suggests that this dimerization depends on the residence time of monomeric UV-DDB on DNA, independent of its specific association with damage. The observation of sliding UV-DDB (K244E) on DNA containing lesions suggests that mutation of the critical K244 leads to an inability of the mutant DDB2 to conformationally proofread the DNA for damage.

Jumping as a Mechanism for Target Search: Implications for Search. The role of UV-DDB in vivo is to recognize photoproducts in genomic DNA. The organization of genomic DNA into nucleosomes and other chromatin higher-order structures may occlude sites of damage and serve as a barrier to DNA damage search. How might the recognition of these lesions proceed inside living cells? Our work provides direct evidence for a 3D search mechanism for DNA damage search by UV-DDB. The interaction of a small population of UV-DDB in real time was consistent with jumping from one λ-DNA molecule to another in our single-molecule DNA tightrope assay (Movie S1). Of the total DNA-bound WT UV-DDB molecules observed, less than 2% showed perceptible linear diffusion. Importantly, because

our spatial resolution is about 100 bp, we cannot rule out short-range 1D sliding (*SI Materials and Methods*, section 1.3). These findings are consistent with a recent report on the promoter search used by *Escherichia coli* RNA polymerase, which posits that target search is favored via a 3D diffusion mode over a facilitated mode of diffusion in a concentration-dependent manner (35, 48). Recently it has been demonstrated that nucleosomal core particles containing site-specific UV photoproducts exhibit spontaneous unwrapping of the DNA, providing access to damaged DNA (49). Rapid sampling of exposed DNA by a 3D search mechanism minimizes the need to overcome obstacles to 1D sliding, such as other DNA-binding proteins and higher-order chromatin organization. Confinement of UV-DDB in higher-order structures of chromatin may confer the ability to repeatedly sample nucleosomal DNA for damage. Such a 3D search mechanism coupled with short-range (<100-bp) diffusion may serve as an effective strategy to interrogate nucleosomal, as well as linker DNA in chromatin. Because UV-DDB exists in about 1.8×10^5 copies per human cell nucleus (translating to an in vivo concentration of the order of a few hundred nanomolars) (14), we propose that UV-DDB rapidly surveys the genome using 3D diffusion and proofreads the DNA for damaged bases in discrete kinetic steps in an excess of undamaged DNA. How the presence of histones and the configuration of DNA in nucleosomes affects the kinetics of binding remains to be investigated.

Our previous work revealed that full-length human UV-DDB dimerizes on DNA at sites of damage via the N terminus of DDB2 (26). Here, we demonstrated that these dimers of UV-DDB are long-lived on DNA, with residence times greater than 900 s. However, the residence of UV-DDB on DNA inside living cells is likely determined by posttranslational modifications of the N terminus of DDB2, which is involved in this dimerization. Autoubiquitination at lysines in the N terminus of DDB2 (18) may disrupt its secondary structure (26) and dismantle the highly stable UV-DDB dimer observed in this work. Recent reports have identified that the N terminus of DDB2 is also PARylated in vivo in response to UV damage, resulting in stabilization of UV-DDB on damaged chromatin (50, 51). How posttranslational modifications such as phosphorylation (52), SUMOylation (53), ubiquitylation (21), and PARylation (50, 51), as well as interacting partners such as XPC and XPA (21, 54, 55), may regulate the dimerization and lifetimes of the kinetic intermediates identified in this work need to be further investigated.

Our work reveals that even a relatively simple step of damage binding is highly regulated even in the absence of protein partners and supports the hypothesis that multiple layers of damage recognition and verification are needed before the final commitment to repair DNA is made (56). Previous work has suggested that damage verification in NER proceeds via an ATP-dependent kinetic proofreading mechanism performed by the XPD helicase in TFIIH (57, 58). Here, we propose that before kinetic proofreading by TFIIH, damage recognition by UV-DDB proceeds via the formation of multiple repair intermediates in a kinetic cascade, using a mechanism which resembles conformational proofreading (31). Further, we hypothesize that conformational proofreading is a common feature of damage recognition in the absence of energy consumption and is also used by XPC to discriminate damage. In this regard, it is interesting to note that conformational and kinetic proofreading mechanisms have been found to operate together for highly specific recognition of homologous sequences during homologous recombination (59, 60). We believe that this synergy of damage detection mechanisms is required for the successful navigation of the complex kinetic and thermodynamic landscape of DNA damage recognition, which achieves high specificity by rejecting nonoptimal repair intermediates. Future studies will help reveal whether the combination of proofreading mechanisms is a universal feature of DNA damage recognition.

Materials and Methods

Biological Reagents. UV-DDB was purified as described previously (26). Various strategies were explored for QD conjugation and these are described in detail in *SI Materials and Methods*, section 1. The QD conjugation strategy described in ref. 29 was used to conjugate UV-DDB (His-DDB1/DDB2) to the penta-His–biotinylated conjugated (Qiagen; His-Ab). SA-QDs (Invitrogen) were conjugated to penta-His–biotinylated conjugated (Qiagen) in a molar ratio of 1:5 for 20 min at room temperature (RT). Following this, the His-Ab QD conjugates were incubated with UV-DDB so as to obtain a final molar ratio of UV-DDB:His-Ab:QD = 1:5:1.

DNA Tightrope Assay. The DNA tightrope assay was performed as described before (28). Custom flow chambers were constructed essentially as described before (28). Poly-L-lysine hydrobromide [MW (molecular weight) > 300,000; Wako Pure Chemicals]-coated silica beads (5 μm; Polysciences Inc.) were deposited on a PEGylated (mPEG-succinimidyl valerate, MW 5,000; Laysan Bio, Inc.) glass coverslip in a flow chamber. Following this step, DNA substrates were elongated between beads using the protocol developed previously. Imaging was performed in either low-salt buffer [150 mM NaCl, 50 mM Hepes 7.5, 100 mM DTT, and 1 mg/mL BSA (Roche)] or high-salt buffer [1 M NaCl, 50 mM Hepes 7.5, 100 mM DTT, 1 mg/mL BSA (Roche)] with 0.8 nM of either QD UV-DDB or QD UV-DDB (K244E). Experiments on undamaged and UV-damaged DNA were performed with bacteriophage λ-DNA (New England Biolabs). UV damage was introduced into bacteriophage λ-DNA by irradiating the DNA with UV-C at a dose of 20 $J \cdot m^{-2}$ and was quantified using qPCR. UV-damaged DNA substrates contained on average one photoproduct in 2,200 bp of DNA (see *SI Materials and Methods*, section 2 for details). DNA substrates containing defined lesions were prepared by introducing a defined lesion in a plasmid as described before (40) and were linearized before tandem ligation to obtain long DNA substrates as described in the *SI Materials and Methods*, section 5.

Oblique-Angle Fluorescence Imaging. Oblique-angle fluorescence imaging was performed using a Nikon Ti eclipse base with a 100× TIRF objective with 1.45 N.A. Flow cells were illuminated by a 488-nm laser. Emissions from QDs were separated using emission filters (Chroma) mentioned here: 655 nm (640/20 or 700/75), 705 nm (700LP or 700/75), 605 nm (600/50), 585 nm (600/50) and 565 nm (535/50) and 520 nm using a (520/40). Images were acquired using Nikon Elements Ar (4.11.00) with a temporal resolution of 100 ms with a laser power of 1–2 mW at the back focal plane of the objective using an Andor Neo sCMOS camera. Lifetime measurements were performed with the Qdot 655 nm streptavidin conjugate.

Data Analysis. Movies captured with NIS-Elements Ar software were exported as a stack of Tagged Image File Format (TIFF) files. TIFF files were further analyzed using ImageJ software (http://imagej.nih.gov/ij/). Kymographs were generated for particles and lifetimes were measured from these kymographs as described previously (28). Diffusion constants were calculated from kymographs as described in *SI Materials and Methods*, sections 4.2 and 6.3.

Pull-Down Experiment. Details of DNA substrates and conditions of the pull-down experiment are presented in *SI Materials and Methods*, section 6.1.

AFM. Samples for AFM imaging in air were prepared by incubating 25 nM nondamaged 517-bp DNA with 50 nM UV-DDB (K244E) for 10 min at RT. Imaging conditions and deposition are described in *SI Materials and Methods*, section 6.4.

ACKNOWLEDGMENTS. We thank Greg Gibson for help with troubleshooting related to imaging; Arthur S. Levine for support; Neil Kad for critically reading the manuscript; Guillermo Romero, Marcel Bruchez, and Roger Hendrix for helpful discussions; Jacob Piehler for providing the biotinylated trisnitrilotriaceticacid compound; and Chunwei Du and Peggy Hsieh for assistance with pSCW01. This work was made possible through the generous support of the University of Pittsburgh Cancer Institute Cancer Center Support Grant P30 CA 047904 and from National Institutes of Health Grant 1R01ES019566.

1. Sugasawa K (2011) Multiple DNA damage recognition factors involved in mammalian nucleotide excision repair. *Biochemistry (Mosc)* 76(1):16–23.
2. Lange SS, Takata K, Wood RD (2011) DNA polymerases and cancer. *Nat Rev Cancer* 11(2):96–110.
3. Hanawalt PC, Spivak G (2008) Transcription-coupled DNA repair: Two decades of progress and surprises. *Nat Rev Mol Cell Biol* 9(12):958–970.
4. Pfeifer GP, You YH, Besaratinia A (2005) Mutations induced by ultraviolet light. *Mutat Res* 571(1-2):19–31.
5. Tang JY, Hwang BJ, Ford JM, Hanawalt PC, Chu G (2000) Xeroderma pigmentosum p48 gene enhances global genomic repair and suppresses UV-induced mutagenesis. *Mol Cell* 5(4):737–744.
6. Aboussekhra A, et al. (1995) Mammalian DNA nucleotide excision repair reconstituted with purified protein components. *Cell* 80(6):859–868.
7. Gillet LC, Schärer OD (2006) Molecular mechanisms of mammalian global genome nucleotide excision repair. *Chem Rev* 106(2):253–276.
8. Wakasugi M, et al. (2001) Damaged DNA-binding protein DDB stimulates the excision of cyclobutane pyrimidine dimers in vitro in concert with XPA and replication protein A. *J Biol Chem* 276(18):15434–15440.
9. Wood RD (1996) DNA repair in eukaryotes. *Annu Rev Biochem* 65:135–167.
10. DiGiovanna JJ, Kraemer KH (2012) Shining a light on xeroderma pigmentosum. *J Invest Dermatol* 132(3 Pt 2):785–796.
11. Nichols AF, Ong P, Linn S (1996) Mutations specific to the xeroderma pigmentosum group E Ddb- phenotype. *J Biol Chem* 271(40):24317–24320.
12. Rapić-Otrin V, et al. (2003) True XP group E patients have a defective UV-damaged DNA binding protein complex and mutations in DDB2 which reveal the functional domains of its p48 product. *Hum Mol Genet* 12(13):1507–1522.
13. Iwai S, et al. (1999) Benzimidazolium triflate-activated synthesis of (6-4) photoproduct-containing oligonucleotides and its application. *Nucleic Acids Res* 27(11):2299–2303.
14. Wittschieben BO, Iwai S, Wood RD (2005) DDB1-DDB2 (xeroderma pigmentosum group E) protein complex recognizes a cyclobutane pyrimidine dimer, mismatches, apurinic/apyrimidinic sites, and compound lesions in DNA. *J Biol Chem* 280(48): 39982–39989.
15. Reardon JT, et al. (1993) Comparative analysis of binding of human damaged DNA-binding protein (XPE) and Escherichia coli damage recognition protein (UvrA) to the major ultraviolet photoproducts: T[c,s]T, T[t,s]T, T[6-4]T, and T[Dewar]T. *J Biol Chem* 268(28):21301–21308.
16. Groisman R, et al. (2003) The ubiquitin ligase activity in the DDB2 and CSA complexes is differentially regulated by the COP9 signalosome in response to DNA damage. *Cell* 113(3):357–367.
17. Luijsterburg MS, et al. (2007) Dynamic in vivo interaction of DDB2 E3 ubiquitin ligase with UV-damaged DNA is independent of damage-recognition protein XPC. *J Cell Sci* 120(Pt 15):2706–2716.
18. Fischer ES, et al. (2011) The molecular basis of CRL4DDB2/CSA ubiquitin ligase architecture, targeting, and activation. *Cell* 147(5):1024–1039.
19. Kapetanaki MG, et al. (2006) The DDB1-CUL4ADDB2 ubiquitin ligase is deficient in xeroderma pigmentosum group E and targets histone H2A at UV-damaged DNA sites. *Proc Natl Acad Sci USA* 103(8):2588–2593.
20. Guerrero-Santoro J, et al. (2008) The cullin 4B-based UV-damaged DNA-binding protein ligase binds to UV-damaged chromatin and ubiquitinates histone H2A. *Cancer Res* 68(13):5014–5022.
21. Sugasawa K, et al. (2005) UV-induced ubiquitylation of XPC protein mediated by UV-DDB-ubiquitin ligase complex. *Cell* 121(3):387–400.
22. Lan L, et al. (2012) Monoubiquitinated histone H2A destabilizes photolesion-containing nucleosomes with concomitant release of UV-damaged DNA-binding protein E3 ligase. *J Biol Chem* 287(15):12036–12049.
23. Wang H, et al. (2006) Histone H3 and H4 ubiquitylation by the CUL4-DDB-ROC1 ubiquitin ligase facilitates cellular response to DNA damage. *Mol Cell* 22(3):383–394.
24. Takedachi A, Saijo M, Tanaka K (2010) DDB2 complex-mediated ubiquitylation around DNA damage is oppositely regulated by XPC and Ku and contributes to the recruitment of XPA. *Mol Cell Biol* 30(11):2708–2723.
25. Rapić-Otrin V, McLenigan MP, Bisi DC, Gonzalez M, Levine AS (2002) Sequential binding of UV DNA damage binding factor and degradation of the p48 subunit as early events after UV irradiation. *Nucleic Acids Res* 30(11):2588–2598.
26. Yeh JI, et al. (2012) Damaged DNA induced UV-damaged DNA-binding protein (UV-DDB) dimerization and its roles in chromatinized DNA repair. *Proc Natl Acad Sci USA* 109(41):E2737–E2746.
27. Hughes CD, et al. (2013) Real-time single-molecule imaging reveals a direct interaction between UvrC and UvrB on DNA tightropes. *Nucleic Acids Res* 41(9): 4901–4912.
28. Kad NM, Wang H, Kennedy GG, Warshaw DM, Van Houten B (2010) Collaborative dynamic DNA scanning by nucleotide excision repair proteins investigated by single-molecule imaging of quantum-dot-labeled proteins. *Mol Cell* 37(5):702–713.
29. Dunn AR, Kad NM, Nelson SR, Warshaw DM, Wallace SS (2011) Single Qdot-labeled glycosylase molecules use a wedge amino acid to probe for lesions while scanning along DNA. *Nucleic Acids Res* 39(17):7487–7498.
30. Lin J, et al. (2014) TRF1 and TRF2 use different mechanisms to find telomeric DNA but share a novel mechanism to search for protein partners at telomeres. *Nucleic Acids Res* 42(4):2493–2504.
31. Savir Y, Tlusty T (2007) Conformational proofreading: The impact of conformational changes on the specificity of molecular recognition. *PLoS ONE* 2(5):e468.
32. Kad NM, Van Houten B (2012) Dynamics of lesion processing by bacterial nucleotide excision repair proteins. *Prog Mol Biol Transl Sci* 110:1–24.
33. Gorman J, Greene EC (2008) Visualizing one-dimensional diffusion of proteins along DNA. *Nat Struct Mol Biol* 15(8):768–774.
34. von Hippel PH, Berg OG (1989) Facilitated target location in biological systems. *J Biol Chem* 264(2):675–678.
35. Wang F, et al. (2013) The promoter-search mechanism of Escherichia coli RNA polymerase is dominated by three-dimensional diffusion. *Nat Struct Mol Biol* 20(2): 174–181.
36. Resch-Genger U, Grabolle M, Cavaliere-Jaricot S, Nitschke R, Nann T (2008) Quantum dots versus organic dyes as fluorescent labels. *Nat Methods* 5(9):763–775.
37. Bruchez MP (2011) Quantum dots find their stride in single molecule tracking. *Curr Opin Chem Biol* 15(6):775–780.
38. Tycon MA, Dial CF, Faison K, Melvin W, Fecko CJ (2012) Quantification of dye-mediated photodamage during single-molecule DNA imaging. *Anal Biochem* 426(1):13–21.
39. Kastantin M, Schwartz DK (2013) Identifying multiple populations from single-molecule lifetime distributions. *ChemPhysChem* 14(2):374–380.
40. Geng H, et al. (2011) In vitro studies of DNA mismatch repair proteins. *Anal Biochem* 413(2):179–184.
41. Alekseev S, et al. (2008) Cellular concentrations of DDB2 regulate dynamic binding of DDB1 at UV-induced DNA damage. *Mol Cell Biol* 28(24):7402–7413.
42. El-Mahdy MA, et al. (2006) Cullin 4A-mediated proteolysis of DDB2 protein at DNA damage sites regulates in vivo lesion recognition by XPC. *J Biol Chem* 281(19): 13404–13411.
43. Wang QE, et al. (2005) Cellular ubiquitination and proteasomal functions positively modulate mammalian nucleotide excision repair. *Mol Carcinog* 42(1):53–64.
44. Scrima A, et al. (2008) Structural basis of UV DNA-damage recognition by the DDB1-DDB2 complex. *Cell* 135(7):1213–1223.
45. Eyal E, Yang LW, Bahar I (2006) Anisotropic network model: Systematic evaluation and a new web interface. *Bioinformatics* 22(21):2619–2627.
46. Hoskins AA, et al. (2011) Ordered and dynamic assembly of single spliceosomes. *Science* 331(6022):1289–1295.
47. Hopfield JJ (1974) Kinetic proofreading: A new mechanism for reducing errors in biosynthetic processes requiring high specificity. *Proc Natl Acad Sci USA* 71(10): 4135–4139.
48. Friedman LJ, Mumm JP, Gelles J (2013) RNA polymerase approaches its promoter without long-range sliding along DNA. *Proc Natl Acad Sci USA* 110(24):9740–9745.
49. Duan MR, Smerdon MJ (2010) UV damage in DNA promotes nucleosome unwrapping. *J Biol Chem* 285(34):26295–26303.
50. Pines A, et al. (2012) PARP1 promotes nucleotide excision repair through DDB2 stabilization and recruitment of ALC1. *J Cell Biol* 199(2):235–249.
51. Robu M, et al. (2013) Role of poly(ADP-ribose) polymerase-1 in the removal of UV-induced DNA lesions by nucleotide excision repair. *Proc Natl Acad Sci USA* 110(5): 1658–1663.
52. Zhao Q, et al. (2008) The p38 mitogen-activated protein kinase augments nucleotide excision repair by mediating DDB2 degradation and chromatin relaxation. *J Biol Chem* 283(47):32553–32561.
53. Tsuge M, et al. (2013) SUMOylation of damaged DNA-binding protein DDB2. *Biochem Biophys Res Commun* 438(1):26–31.
54. Wakasugi M, et al. (2009) Physical and functional interaction between DDB and XPA in nucleotide excision repair. *Nucleic Acids Res* 37(2):516–525.
55. Otrin VR, McLenigan M, Takao M, Levine AS, Protić M (1997) Translocation of a UV-damaged DNA binding protein into a tight association with chromatin after treatment of mammalian cells with UV light. *J Cell Sci* 110(Pt 10):1159–1168.
56. Naegeli H, Sugasawa K (2011) The xeroderma pigmentosum pathway: Decision tree analysis of DNA quality. *DNA Repair (Amst)* 10(7):673–683.
57. Reardon JT, Sancar A (2004) Thermodynamic cooperativity and kinetic proofreading in DNA damage recognition and repair. *Cell Cycle* 3(2):141–144.
58. Mathieu N, Kaczmarek N, Naegeli H (2010) Strand- and site-specific DNA lesion demarcation by the xeroderma pigmentosum group D helicase. *Proc Natl Acad Sci USA* 107(41):17545–17550.
59. De Vlaminck I, et al. (2012) Mechanism of homology recognition in DNA recombination from dual-molecule experiments. *Mol Cell* 46(5):616–624.
60. Sagi D, Tlusty T, Stavans J (2006) High fidelity of RecA-catalyzed recombination: A watchdog of genetic diversity. *Nucleic Acids Res* 34(18):5021–5031.

Supporting Information

Ghodke et al. 10.1073/pnas.1323856111

SI Materials and Methods

1. Target Search and Conjugation Strategies. ***1.1. Target search.*** DNA-binding proteins may locate their target sites on DNA either by 3D diffusion in solution followed by productive collisions or any number of facilitated modes of diffusion on the DNA such as 1D diffusion, hopping, intersegmental transfer, and directed motion (Fig. S1*A*).

1.2. Strategies to conjugate UV-DDB to streptavidin-coated quantum dots. Our purification strategies use dual FLAG and His-tags to isolate the UV-DDB complex for the following constructs of UV-DDB: $^{\text{FLAG-His}}$DDB1/DDB2, $^{\text{His}}$DDB1/$^{\text{FLAG}}$DDB2, and DDB1/$^{\text{FLAG-His}}$DDB2 (1). Based on these constructs, we identified three different strategies to conjugate UV-DDB to streptavidin-coated quantum dots (SA-QDs), presented below. Conjugation was performed in low-salt buffer.

1.2.1. Using the biotinylated trisnitrilotriaceticacid compound. We first tested the conjugation strategy involving a biotinylated trisnitrilotriaceticacid (BT-NTA) compound (2). We assayed DNA binding of QD-conjugated UV-DDB ($^{\text{FLAGHis}}$DDB1-DDB2) to AP36 dsDNA substrate by the use of an agarose based EMSA (3). AP36 dsDNA substrate was prepared by hybridizing 5′ ^{32}P-radiolabeled 36-mer RC36 (5′ - TTT GAC TCC CAT GGA CTC GCT GCA GGA ATG ACT CGG) to a 36-mer containing an abasic site analog [Int dSpacer containing a 1′,2′-Dideoxyribose which generates a stable abasic site analog; integrated DNA technologies (IDT)] at a defined site (5′ - CCG AGT CAT TCC TGC AGC G/idSp/G TCC ATG GGA GTC AAA - 3′). Binding reactions were performed for 20 min at room temperature (RT) in low-salt buffer and separated over a 1% agarose gel for 50 min at 100 V on ice. Gels were dried for 1 h at 65 °C. Using the BT-NTA compound, we found that under the conditions tested, UV-DDB exhibits a supershift in DNA binding upon conjugation with BT-NTA; however, this supershift is lost upon conjugation to QDs. BT-NTA–conjugated QD UV-DDB exhibits a small supershift, but also leads to a significant loss of DNA-damage-binding ability, suggesting that the short length of the BT-NTA linker to the QD inhibits the stable binding of UV-DDB to DNA through steric hindrance.

1.2.2. Using the FLAG antibody sandwich approach. We next tested an antibody sandwich approach using a primary anti-FLAG antibody and IgG-coated QDs to conjugate $^{\text{FLAG-His}}$DDB1/DDB2 to QDs (4). We found that QD UV-DDB exhibits a measurable supershift in the agarose EMSA corresponding to DNA-bound QD FLAG Ab UV-DDB complexes on 177-bp UV-irradiated DNA. Evidence for these complexes was also observed by atomic force microscopy (AFM) when QD FLAG Ab UV-DDB was incubated with UV-irradiated 517-bp DNA containing on average one lesion per fragment (Fig. S1*B*).

1.2.3. Characterizing binding activity using the His-Ab conjugation strategy. We performed EMSAs to measure the binding of His-Ab–conjugated (5) QD UV-DDB to a AP36 containing an abasic site analog which has previously been demonstrated to be a robust substrate for UV-DDB (Fig. S1*C*) (1). QD conjugation was performed as described previously (5). First SA QDs were incubated with His-Ab in the indicated ratio for 30 min at RT, followed by incubation with appropriate amounts of UV-DDB for an additional 30 min to obtain the indicated molar ratio. Binding reactions with 5′ ^{32}P-labeled AP36 dsDNA substrate were performed for 20 min at RT in low-salt buffer and separated over a 1% agarose gel for 50 min at 100 V on ice. Gels were dried for 1 h at 65 °C followed by autoradiography. We found that His-Ab–conjugated UV-DDB ($^{\text{FLAGHis}}$DDB1/DDB2) demonstrated a measurable supershift corresponding to UV-DDB-His-Ab-QD:DNA complexes (Fig. S1*C*, lane 6). Additionally, no nonspecific binding of either the His-Ab or QDs binding to DNA was detected (Fig. S1*C*, lanes 3 and 4). We also tested our other UV-DDB constructs ($^{\text{His}}$DDB1/$^{\text{FLAG}}$DDB2 and DDB1/$^{\text{FLAGHis}}$DDB2) and found that in all cases, DNA-binding activity was retained (Fig. S1*C*, lanes 7–9 and 10–12, respectively). Further, we tried different UV-DDB:His-Ab:QD ratios such as 1:5:1, 1:5:2.5, and 1:5:5 and found robust supershifts for the QD-conjugated DNA-bound complex under our incubation conditions (Fig. S1*D*). However, we used a ratio of 1:5:1 for our experiments, because under these conditions the biotin binding sites on the SA-QDs are completely saturated (5).

The His-Ab-SA-QD strategy was found to be robust and we therefore decided to proceed with this strategy for observing the protein–DNA interactions in real time in the DNA tightrope assays. Importantly, UV-DDB is a tightly associated complex of DDB1 and DDB2 and previous reports have reported similar diffusion constants for the complex containing DDB1 and DDB2 when either subunit was fluorescently tagged inside living cells (6). Given these results, we believe that conjugating the DDB1 subunit with QDs serves as an accurate reporter for the behavior of DDB2 on DNA.

For imaging in the DNA tightrope assay, QD UV-DDB or UV-DDB (K244E) was conjugated according to the protocol described previously (5) and diluted 1:100 to a final concentration of 0.8 nM in low-salt buffer (150 mM NaCl, 50 mM Hepes 7.5, 100 mM DTT, and 1 mg/mL BSA).

1.2.4. Imaging in the absence of YOYO-1. Consistent with a recent report, we observed shattering of DNA tightropes incubated with YOYO-1 during imaging, presumably via the formation of single-strand breaks followed by double-strand breaks (7) limiting our observation times to less than 60 s. To enable long observation times for UV-DDB binding to DNA, the use of YOYO-1 was avoided in these experiments.

1.3. Calculating the positional accuracy and localization precision. Positional accuracy was calculated for 605-nm QD (bound to biotin on DNA containing the defined lesion substrates) in each frame as follows: First, a line was drawn across the center of the fluorophore to obtain the intensity profile. The intensity profile was then fit to a Gaussian fit, to obtain the mean position and its SD(s). Using the intensity profile, the corresponding photon count profile was calculated as

$$N = (\text{Count} - \text{bias offset}) \times \frac{S}{\text{QE}}$$

where "Count" is the gray level from imaging software, "bias offset" = 100, S is the sensitivity (electrons/count), and QE is the quantum efficiency (electrons/photon).

The total number of photons (N_p) was calculated by integrating the area under the photon count profile corrected for the background. The SD in the background intensity was used to calculate the value of b which corresponds to the SD in the background photon count. These values were then used to calculate the positional accuracy (σ) using the formula described previously (8):

$$\sigma = \sqrt{\left(\frac{s^2}{N_p} + \frac{a^2}{12N_p} + \frac{4s^3b^2\sqrt{\pi}}{aN_p^2}\right)}.$$

For our instrument, the pixel size a was 46 nm. For a typical QD, s = 193 nm, N_p = 5,700, and b = 24. Mean positional accuracy

was calculated for each 605 nm QD bound to biotin on the defined lesion substrate ($n = 16$), by taking the average of the positional accuracy measurements in each "on" frame in a time series of 200 frames. These mean positional accuracies were found to lie in the range from 2 to 11 nm (depending on the brightness of the QD). The average and SD for these 16 QDs was found to be 6 ± 3 nm.

The localization precision of a QD over an entire time series was calculated as described previously (9, 10). To calculate the localization precision for the kth single QD over an entire time series [index $i = (1, \ldots, N_k)$, where N_k represents the total number of "on" frames] the mean position for the QD was obtained by averaging the center of the 2D Gaussian fit to the intensity profile obtained using the Spottracker2D plugin in ImageJ. The mean position of a QD in over the entire movie was calculated as

$$\left\{\langle x_{k,c}\rangle, \langle y_{k,c}\rangle\right\} = \frac{1}{N_k}\sum_{i=1}^{N_k}\left\{x_{k,i}y_{k,i}\right\}.$$

The SD in the mean position was then calculated as below:

$$\left\{\langle \Delta_x^2\rangle, \langle \Delta_y^2\rangle\right\} = \frac{1}{N_k - 1}\sum_{i=1}^{N_k}\left\{\left(x_{k,i} - \langle x_{k,c}\rangle\right)^2, \left(y_{k,i} - \langle y_{k,c}\rangle\right)^2\right\}.$$

The average uncertainty and its SE were found to be 36 ± 3 nm along x axis and 33 ± 2 nm along y axis. This value represents the uncertainty in the position of a QD conjugated to a biotin on the DNA tightrope arising from underlying fluctuations of the DNA, background stage drifts, and thermal fluctuations.

2. Generation and Measurement of UV Damage in λ-DNA Substrates. Exposure of DNA to UV radiation leads to primarily to two types of photolesions, pyrimidine(6–4)pyrimidone photoproducts [(6–4) photoproducts] and cyclobutane pyrimidine dimers. In this approach, a UV-C lamp (254 nm) was used to generate randomly UV-damaged λ-DNA. UV-induced damage in DNA was quantified by qPCR developed by our laboratory, essentially as previously described using the GeneAmp XL PCR Kit (Applied Biosystems; catalog no. N8080193) (11). A 12.5-kb fragment of λ-DNA (New England Biolabs) was amplified between nucleotides 26,890 and 39,488 (forward primer: 5′ CCA ACC ATC TGC TCG TAG GAA TGC 3′; reverse primer: 5′AGT TGG GTC CAC TTA TCG CGG AGT 3′, IDT). Cycle conditions for amplification of 15 ng of λ-DNA template were 1 min 30 s for 75 °C, followed by addition of polymerase, 94 °C for 1 min, 94 °C for 15 s, 64 °C for 12 min (11 cycles), final extension: 72 °C 10 min. Amplification of damaged DNA was measured relative to mock irradiated λ-DNA that was treated similarly. Final product was visualized by gel electrophoresis with ethidium bromide staining. PCR product concentrations were measured using PicoGreen fluorescent DNA-binding dye (Molecular Probes; Quant-iT PicoGreen dsDNA assay kit, catalog no. P7581). Three microliters of PCR product were diluted in a 1:200 dilution of PicoGreen in Tris pH 8.0, 10 mM, EDTA 1.0 mM and relative fluorescence units were calculated for each sample. Further, these samples were converted to an absolute DNA concentration by using a standard curve created from measuring the relative fluorescence units for different concentrations of λ-HindIII standards. Fifty percent of controls were performed with untreated, undamaged λ-DNA. A dose–response curve relating the number of UV lesions in the λ-DNA fragment as a function of UV dose was obtained as follows: lesions/λ-DNA = 1.0958 UV-dose ($J{\cdot}m^{-2}$) – 0.0136, $R^2 = 0.9997$, and $n = 2$ with each experiment performed in duplicate (Fig. S2*A*). UV-damaged DNA containing one UV-induced photoproduct in 2,200 bp of DNA was used in the DNA tightrope assay.

3. Lifetime Analysis. ***3.1. System definitions.***

3.1.1. Describing Poisson processes for a system shuttling reversibly between two states. Consider a system which reversibly shuttles between two observable states S_i and S_k. Here, we define a state as a configuration of the biomolecule in consideration. The differences in the states arise from differences in the spatial positions of the constituent atoms in the macromolecules which interact with each other. Assume that the decay from the ith state the kth state (and vice versa) is experimentally measurable.

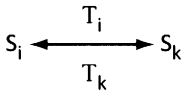

For a Poisson process (T_i), the escape from the S_i state to the S_k state is given by $T_i \equiv exp\{-k_{d,i}t\}$, where, $k_{d,i}$ represents the rate constant for the decay process and the mean lifetime for the S_i state is obtained as $\tau_i = k_{d,i}^{-1}$. A similar (T_k) process can be described for the reverse reaction if the process is a Poisson process.

3.1.2. Cumulative residence time distribution analysis for transients on DNA. Dissociation kinetics of a population of proteins bound to DNA as a single intermediate may be described by a Poisson process. For a heterogeneous population of intermediates let the number of molecules of the population participating in the ith kinetic intermediate (described by the ith Poisson process $T_i \equiv exp\{-k_{d,i}t\}$, be given by

$$n_i(t) = a_i T_i.$$

Here, $n_i(t)$ represents the number of molecules of the ith kinetic intermediate remaining on the DNA as a function of time, starting with an initial population of a_i observations. In general, the dissociation kinetics of populations consisting of N_p distinct Poisson processes are described by

$$n(t) = \sum_{i=1}^{N_p} a_i e^{-k_{d,i}t}.$$

Here, $n(t)$ represents the total number of molecules which remain associated with the DNA as a function of time for all of the different kinetic intermediates taken together. The normalized fraction, $f(t)$ represents the cumulative residence time distribution (CRTD).

3.2. Best fit of the experimental data to the CRTD. The CRTD was fit to a sum of N_p Poisson processes starting with $n = 1, \ldots, N_p$. Fit parameters for double ($N_p = 2$) and triple ($N_p = 3$) are provided in the Table S1 below. Log-log plots for the experimental data and double exponential fit (dashed blue line) and triple exponential fits (solid, red) are presented in Fig. S3 *A* and *B* for undamaged and damaged DNA. From these plots, it is evident that all of the features of the data are only captured when $N_p = 3$. Because SSE/df was found to be smaller for $N_p = 3$, we proceeded with fitting the population to 3 Poisson processes (Table S1).

3.3. Fit parameters for exponential fits to the experimental data for transient binding to undamaged as well as damaged DNA. The fraction of molecules participating in each Poisson process was calculated by normalizing the contribution from that process and requiring that the initial condition that the sum of all fractions of all populations be equal to 1, be met at $t = t_0$, which represents the time at which the first dissociation event occurs.

The fraction of molecules participating in each of the transient binding populations was obtained by normalizing the contribution of the exponential at the start of observation f_i (plotted in Fig. 3 *C* and *D*), i.e.,

$$f_i = \frac{a_i e^{-k_{d,i} t_0}}{\sum_i a_i e^{-k_{d,i} t_0}}.$$

We first identified that the estimates for the amplitudes of the pairs of the decay processes were significantly different from each other ($P < 0.0001$; Table 1). We then normalized the fitted data to obtain the relative fractions of the kinetic intermediates that decay according to the three different processes for transient binding to undamaged vs. UV-damaged DNA.

3.4. A kinetic cascade for damage recognition. Consider the reversible binding of a deformable protein P binding deformable DNA D. Let P_0 and D_0 represent an interconverting ensemble of conformations, which can include within them the P_i and D_i conformations (for $i > 0$). Let $S_i \equiv (P_i,D_i)$ represent an observable state of the protein (in a conformation P_i) bound to the DNA (in a conformation D_i). Here, the term observable is used to denote that the decay from the S_ith DNA-bound state to the S_0 state is measurable as the T_ith process. Note that the individual conformations of the protein or the DNA in the *i*th state may not be experimentally identifiable. In this notation, we do not require that P_i or D_i be unique, only that each of the states S_i is unique.

Additionally, we specify that this interaction of the protein with the DNA is spontaneous and occurs in the absence of an external energy source, and we require only that $\Delta G_{i+1} < \Delta G_i$ from the respective reference unbound states. Consider a binding scheme where each intermediate may either transition to a more stable state or an unstable state along the reaction coordinate with a finite probability. Then a general model for the interaction of protein and DNA may be proposed as follows:

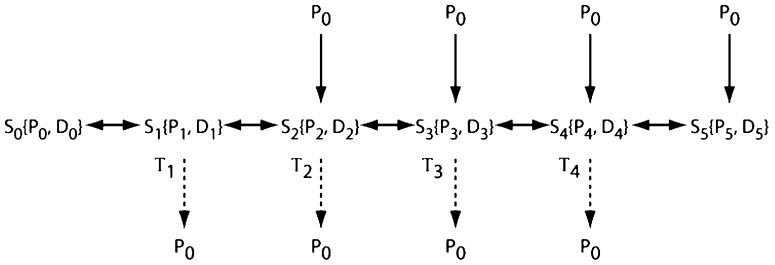

Thus, the complex $S_1 \equiv (P_1,D_1)$ which represents UV-DDB bound with the lowest affinity can either progress to a higher affinity state $S_2 \equiv (P_2,D_2)$ or dissociate to form unbound UV-DDB S_0. Similarly, S_2 will progress to form the higher affinity state $S_3 \equiv (P_3,D_3)$ at a certain rate or escape to the DNA unbound state S_0 possibly by sampling S_1 and so on. In this representation, dashed lines represent an aggregate process, with unspecified intermediate states. Let T_i represent the Poisson process that enables the conversion of UV-DDB from the S_ith to S_0th state, with no specification of the intermediate states sampled in this transition. This reaction scheme describes a kinetic cascade which funnels the protein along a reaction scheme which culminates in the formation of a highly stable complex (P_n) along the reaction coordinate to achieve successful damage recognition with high specificity.

3.5. N(t) vs. t analysis for particles that are initially present and dissociate during observation. For this class of molecules which were bound when first recorded and then dissociated, we can count the number of particles that dissociate as a function of time for either undamaged DNA or UV-damaged DNA. We found that the dissociation of UV-DDB can be fit to an exponential decay of the form

$$N_i(t) = a_i e^{-k_{d,i} t}.$$

With a_i representing the number of particles participating in this decay process at the beginning of observation, presented in Fig. S3 *E* and *F* for undamaged and UV-damaged DNA.

For the case of undamaged DNA, the CRTD was found to best fit a double exponential fit (Fig. S3*E*), one of which was statistically indistinguishable from the $T_{2,ud}$ process ($P = 0.0749$) and the other exponential fit ($T_{4,ud}$) was statistically different from the $T_{3,ud}$ ($P < 0.0001$) process. Parameterization of the CRTDs revealed the presence of the $T_{2,ud}$ process and a new $T_{4,ud}$ process describing the dissociation of bound UV-DDB from undamaged DNA. Similarly, from the CRTDs of UV-DDB dissociating from UV-damaged DNA, a new process ($T_{4,d}$) was identified that was consistent with the $T_{4,ud}$ process. In the case of UV-damaged DNA, the CRTD was dominated by a single exponential (Fig. S3*F*) corresponding to a single process ($T_{4,d}$). Although this exponential was found to be distinct from the $T_{4,ud}$ process ($P < 0.0001$) it was found to possess a decay rate which was very similar to that of the $T_{4,d}$ process. It is likely that the $T_{4,ud}$ and $T_{4,ud}$ processes are identical, and the differences in the values arise from poor estimation of the $T_{4,ud}$ process due to low sample size ($n = 11$).

We wondered if it was possible that the population of molecules dissociating according to the T_4 process represents left over molecules from the T_3 process. The data set of dissociating molecules represents those molecules for which $t_{assoc} \geq \tau$ (where t_{assoc} represents the total time of association; note that $t_{assoc} >$ measured lifetime). We examined the limiting case that $t_{assoc} = \tau$ (i.e., the molecules associated with the DNA at the instant before the start of observation) and plotted the decay of 16 (or 67 in case of UV-damaged DNA; Fig. S3 *G* and *H* for undamaged and UV-damaged DNA, respectively) molecules for the cases where $\tau = \{\tau_{3,d}, \tau_{3,d+}, \tau_{3,d-}\}$ and $\tau = \{\tau_{4,d}, \tau_{4,d+}, \tau_{4,d-}\}$, where $\tau_{i,j+}$ represents the upper limit of the 95% confidence interval (CI) and $\tau_{i,j-}$ represents the lower limit of the 95% CI. In all cases we found no overlap of the curves, consistent with the results of the hypothesis indicating that the T_3 and T_4 processes represent distinct intermediates.

The fraction of molecules participating in the T_4 process was 3.3-fold higher and was calculated as fraction decaying according to T_4 process for damaged DNA (67 of 643) fraction decaying according to T_4 process for damaged DNA (11 of 347). Importantly, this T_4 process is statistically distinguishable from the corresponding T_3 process. These observations reveal the formation of a fourth repair intermediate τ_4 (446.2 or 336.7 s) that binds DNA as a function of DNA damage. Because commercially produced λ DNA has inherent damage, such as abasic sites, some of the long-lived intermediates on the "undamaged" DNA molecules probably represent binding to these types of lesions.

4. Analysis of Persistent Molecules. ***4.1. Population of persistent molecules is enriched on damaged DNA.*** From our previous analyses, we identified that the number of molecules that participate in T_3 and T_4 decay processes for undamaged DNA is 21 and 16, respectively, whereas that for UV-damaged DNA is 87 and 67,

respectively. Using the values of the rate constants measured for these processes, the number of molecules that will survive for 900 s can be calculated to be <1 for the first three cases and four for the last case. In comparison, the total number of persistent molecules was found to be 20 (of 347 observations) for binding to undamaged DNA, and 88 (of 643 observations) for UV-damaged DNA. This tremendous enrichment in the number of persistent molecules strongly suggests that these molecules participate in a decay process (assume a Poisson process T5 with a mean lifetime of τ_5) which is far slower than any of the processes that are measureable in our experiments and the length of the acquisition window in our experiments.

4.2. Persistent UV-DDB slides on DNA at 1 M salt. To eliminate the possibility that the persistent UV-DDB we observed in the DNA tightrope assay were irreversible aggregates of UV-DDB on DNA, we washed the chamber with four chamber volumes of a high-salt buffer (1 M NaCl, 10 mM Hepes 7.5, 1 mg/mL BSA). After the buffer exchange, we observed a significant loss (>90%) of DNA-binding events due to dissociation in the presence of high ionic strength. Of the few molecules that remained on the tightropes, we observed that previously stationary UV-DDB on DNA now performed a rapid 1D random walk on DNA (Movie S1 and Fig. S4*A*).

Diffusion constants describing the motion of UV-DDB on DNA tightropes were calculated by performing single-particle tracking of the diffusive particles (12). Briefly, we generated kymographs of the diffusing particles along the length of the DNA and fit the intensity of the QD to a Gaussian curve, to obtain a mean position of the particle, in each frame. In this way, the mean positions of the particle were obtained as a function of time for the entire duration of observation. From this data, mean square displacements (MSDs) ($\langle \Delta x^2 \rangle$) were calculated for varying time steps (Δt), and a plot of the MSD vs. Δt was generated. The initial slope of the MSD was then fit to

$$\langle \Delta x^2 \rangle = 2Dt + c,$$

where D represents the diffusion coefficient, and c represents a constant reflecting aggregate errors in MSD calculation.

The average diffusivity was found to be 0.21 (±2.1) $\mu m^2/s$ (geometric mean ± geometric SD, where D is the diffusivity, $n = 31$; Fig. S4*B*). Importantly, the mean uncorrected diffusion constants we measured were an order of magnitude greater than the upper limit for rotational diffusion proposed by Schurr (13), suggesting that UV-DDB does not rotationally track the DNA when sliding under conditions of high ionic strength. Further, all of these complexes were found to be stable on DNA for at least the duration of acquisition (120 s), suggesting that these complexes possess a molecular topology which constrains them to the DNA.

5. Long DNA Substrates Containing Defined Lesions. ***5.1. Creation of long DNA substrates containing defined lesions for DNA tightrope assays.*** Oligonucleotides with custom chemical modification were introduced into the pSCW01 plasmid essentially as described before (14). pSCW01 was amplified in DH5α and purified using the Qiafilter Maxiprep kit. Typically, 400 μg of pSCW01 were incubated with 60 μL Nt.BstNbI (10 U/μL; New England Biolabs) Nt.BstNBI for 4h at 55 °C in the presence of 100× complementary displacer oligonucleotides to nick the plasmid at the four adjacent nickase sites (refer to ref. 14 for sequences). Following this, the reaction was inactivated by heating to 85 °C for 10 min followed by annealing to displace the nicked oligonucleotides. An equal volume of the reaction mixture was then added to a 2× solution containing 26% (vol/vol) PEG-8000 in 20 mM $MgCl_2$ followed by centrifugation for 1 h at 4 °C. Precipitated DNA pellet was then washed with ethanol followed by resuspension of the gapped plasmid. Purified gapped plasmid DNA was then incubated with the desired oligo in 3× excess followed by annealing in NEB 4 buffer. After annealing, the reaction was supplanted with 8 mM ATP and ligation was performed by the addition of 5 μL T4 DNA ligase (M0202, 2,000 U/μL; New England Biolabs) to a 400-μL reaction containing 400 ng/μL purified gapped plasmid DNA for 18 h at 16 °C. The reaction was then heated to 65 °C for 20 min to inactivate the T4 DNA ligase and supplemented with XhoI (New England Biolabs) to digest the plasmid DNA containing custom oligonucleotide. Restriction was performed for 2 h at 37 °C followed by inactivation at 85 °C for 20 min. Linearized plasmid DNA containing custom chemical modification (monomer) was then stored at −20 °C until further use. To obtain long DNA substrates for the DNA tightrope assay, 1 μg plasmid DNA monomers was ligated for 15 min at RT in Quickligase buffer with 2 μL T4 DNA ligase (2,000 U/μL).

Using this strategy we were able to make DNA substrates with the following chemical modifications:

Oligo	Sequence
APBiodT	/5Phos/ CCG AGT CAT TCC TGC AGC G/idSp/G TCC ATG GGA GTC AAA /3BiodT/

We were able to efficiently string up APbiodT DNA in the flow chamber. To demonstrate proof of concept that the sites of lesions in long DNA substrates can be marked by QDs, we incubated the flow cell with 10 nM streptavidin-coated 605-nm QDs. These QDs were found to rapidly bind to the DNA molecules stretched between beads and they exhibited a periodic pattern of binding, consistent with our design. We then measured the inter-QD distances between pairs of adjacent QDs bound to the biotin on the introduced oligonucleotide containing the defined lesion in the DNA damage array. These distances were plotted in a histogram which was then fit to a multiple Gaussian fit (up to three terms). We found that 46.7% of inter-QD distances on these DNA damage arrays were 0.697 μm apart [95% CI: (0.6899, 0.7044)], 37.8% were 1.348 μm [CI (1.336, 1.359)], and 8.9% were 2.076 μm [95% CI: (2.022, 2.131)] apart (Fig. S5*B*). The measured distances between adjacent QDs on DNA agree very well with the predicted distances between two QDs if they are one (0.65-μm), two (1.30-μm), or three (1.95-μm) plasmid lengths apart (Fig. S5*A*). By measuring the inter-QD distances for adjacent pairs, we found that 85% of the QDs were either one or two plasmid lengths apart (Fig. S5*A*). We believe that the missing sites reflect a lack of QD conjugation or dark QD rather than sites where the oligonucleotide is not incorporated, as restriction digests of the parental damage engineered plasmid indicated that >99% had the oligonucleotide correctly incorporated. These data demonstrate that DNA damage can be introduced and specifically marked in these DNA tightrope substrates efficiently.

5.2. Colocalization experiments involving long DNA substrates containing defined lesions. Experiments targeting the observation of colocalization of QD-conjugated UV-DDB with sites of lesions marked with QDs were performed in low-salt buffer (150 mM NaCL, 50 mM Hepes 7.5, 100 mM DTT, and 1 mg/mL BSA) supplemented with 20 nM biotin. In the experiments presented here, the channel corresponding to QDs on the DNA damage arrays was imaged at a lower frequency (1 in 30 frames), whereas the channel corresponding to QD-conjugated UV-DDB was imaged at 10 frames per second (fps).

5.3. Electrophoretic mobility shift assay to determine extent of binding of UV-DDB to biodT. Because we used biodT labeling to mark the damaged sites in the DNA tightrope damage arrays, a confounding problem could occur if UV-DDB recognized biodT and bound avidly to biodT containing DNA. To identify whether

UV-DDB recognizes biodT in DNA as a lesion, we performed electrophoretic mobility shift assays with the following substrates:

Undamaged top strand (UD36): /5Phos/ CCG AGT CAT TCC TGC AGC GAG TCC ATG GGA GTC AAA

Damaged top strand with biodT (Bio36): /5Phos/ CCG AGT CAT TCC /iBiodT/GC AGC GAG TCC ATG GGA GTC AAA

Damaged top strand with abasic site: /5Phos/ CCG AGT CAT TCC TGC AGC G/idSp/G TCC ATG GGA GTC AAA

These were hybridized to the fluorescent bottom strand: /56-FAM/ TTT GAC TCC CAT GGA CTC GCT GCA GGA ATG ACT CGG.

Hybridization was performed in 1× hybridization buffer (50 mM NaCl, 10 mM Hepes 7.5); 10 nM of each dsDNA substrate were incubated with UV-DDB at the indicated concentrations in low-salt buffer for 30 min at RT. Substrate concentration was maintained at 10 nM. Binding reactions were analyzed using gel electrophoresis through a native 5% (37.5:1) polyacrylamide gel run at 80 V for 50 min. Under these conditions, we found that on average at 10 nM UV-DDB concentration, 14.2%, 17.6%, and 53.5% of the undamaged, biodT, or AP substrates were bound, respectively. At 20 nM UV-DDB, the bound fractions changed to 23%, 30%, and 99% of the undamaged, biodT, or AP substrates, respectively. A one-way ANOVA revealed significant differences between the bound fractions of UV-DDB bound to undamaged, biodT, and AP DNA probes. A post hoc analysis using the Tukey honestly significant difference test revealed that the differences in binding to the undamaged DNA and DNA containing the biodT lesion were nonsignificant. However, binding to both of these substrates was significantly different from binding to DNA containing the AP lesion with $P < 0.01$ (Fig. S5*C*). These results indicate that UV-DDB does not apparently recognize biodT lesions in DNA with binding to these substrates comparable to binding to undamaged DNA.

6. Characterization of UV-DDB Containing the DDB2 K244E Mutation.

6.1. Pulldown experiment with K244E.

6.1.1. Preparation of DNA substrates. DNA substrates for the pulldown experiment were designed with modifications on both ends. 517-bp DNA was created by amplifying pUC18 using the Dig1890A (5′ - /5DigN/ GGT CTG ACG CTC AGT GGA ACG - 3′, IDT) and Bio1373s (5′ - GGA ACC GGA GCT GAA TGA AG - 3′, IDT) primers to create DNA substrates which can be blocked on either end with streptavidin or anti-digoxigenin antibody. PCR was performed using Pfu ultra with 10 ng pUC18. Cycle conditions for PCR were 94 °C for 5 min (hot start, add polymerase after 2 min), 94 °C for 30 s, 57 °C for 1 min, 72 °C for 1 min (30 cycles) and 72 °C for 7 min. PCR product was separated on a 1% agarose gel to identify homogeneity of amplified product. PCR was then purified using Qiaquick PCR purification kit (catalog no. 28104; Qiagen). Purified DNA was eluted in Tris·Cl pH 8.0 and concentrations of DNA were measured using a Nanodrop. Typical yields for purification were found to be between 50% and 60%.

6.1.2. UV irradiation of 517-bp DNA. UV-damaged DNA was obtained by exposing the purified DNA to a dose of 20 J·m^{-2} at 50 ng·μL^{-1}. DNA damage in 517-bp DNA was quantified using quantitative PCR (qPCR) (11) and was found to occur at a frequency of 1.2 photoproducts per 517-bp fragment from two experiments (15 and 16 cycles) (15).

6.1.3. Conjugation to beads. Bio-517-dig DNA (either mock or UV irradiated) was then incubated with streptavidin-coated magnetic beads (Dynabeads, M-280; Invitrogen) in the presence (4× excess over DNA) or absence of anti-digoxigenin antibody (catalog no. 11 333 062 910; Roche) to get undamaged or UV-damaged DNA bound to beads with either one free end or no free ends while rocking for three overnights at 4 °C. Wild-type (WT) UV-DDB or UV-DDB (K244E) was incubated with DNA bound on beads in 1× binding buffer for 30 min at RT in a reaction volume of 20 μL. In the experiment presented here, the final concentration of the UV-DDB (WT or K244E mutant) was 10 nM and that of DNA on beads was 12.5 nM in a total reaction volume of 20 μL. After binding, the beads were washed with three volumes and resuspended in 21 μL 1× binding buffer and 7 μL 4× lithium dodecyl sulfate buffer. Samples were boiled for 10 min at 95 °C and separated on a 4–12% SDS gradient gel. The gel was subsequently transferred and Western blotting was performed on the various fractions which were probed with α-DDB1 and α-DDB2 antibody.

6.2. Binding of UV-DDB (K244E) to 517-bp DNA. A comparison of percentage of binding events to DNA ends vs. internal sites revealed a preference for ends over internal sites (55% vs. 45%, $n = 410$ binding events; Fig. S6*B*). We observed that UV-DDB (K244E) could bind a single DNA molecule nonspecifically (20%), a single DNA end (6%), two DNA ends (16%), one DNA end and an internal site forming a three-way junction (50%), and two DNA molecules at internal sites forming four-way junctions (9%). Further analysis of the AFM images revealed that 74% of the bound UV-DDB (K244E) participated in binding to two DNA molecules compared with 26% bound to single DNA molecules [$n = 216$ UV-DDB (K244E)-DNA complexes]. Interestingly, dimeric WT UV-DDB was found to bind two DNA helices only 20% of the time (15).

6.3. Measurement of the diffusion constant at low salt. For true Brownian motion describing the diffusion in an isotropic medium, the relationship between the MSD and time is linear. This means, that the displacement of a diffusing particle is a linear function of $\sqrt{t}$. However, it has been observed that in practice, the displacement of a particle does not always exhibit a linear relationship with $\sqrt{t}$, prompting the development of new models for fitting the experimental data. One alternate model suggested in the literature describes a subdiffusive phenomenon (12). In this case, the MSD is related to the diffusion constant as

$$\mathrm{MSD}(n,N) = 2Dt(n)^{\alpha}.$$

Here, α is the anomalous diffusive exponent and for values of $\alpha < 1$, signifies that the diffusive medium is not isotropic.

6.4. Deposition and imaging conditions for AFM. AFM reactions were diluted 1:7 in AFM deposition buffer [25 mM NaOAc, 10 mM $Mg(OAc)_2$, and 25 mM Hepes pH 7.5]. Diluted samples were deposited on freshly cleaved mica (SPI Supply) followed by washing with MilliQ water and drying under a stream of nitrogen gas. AFM images were collected using a MultiModeV microscope (Bruker) using an E scanner in tapping mode in air. Pointprobe plus noncontact/tapping mode silicon probes (PPP-NCL; Agilent) with spring constants of ∼50 Nm^{-1} and resonance frequencies in the range from 150–200 kHz were used. Images were captured at a scan size of 1 μM × 1 μM with a resolution of 512 pixels × 512 pixels at a scan rate of 4 Hz and a target amplitude of 300 mV.

6.5. Measurement of AFM volumes. We have previously developed a correlation between the molecular volume enclosed under a peak in an AFM image and the molecular weight of the protein which enables us to identify the oligomeric state of the protein (16). This approach has been successfully used by us and others to identify the composition and stoichiometry of protein DNA complexes when imaged by AFM. In this work also, we have performed a similar analysis to identify the oligomeric state of UV-DDB (K244E) bound to DNA. Previously (15) we erroneously reported the AFM volume as cubic nanometers, whereas, in reality, it has been calculated as pixels to the power of 2

(pix^2nm). In this work, we have used an updated version of the ImageSXM software and corrected the error, so that henceforth, all of the AFM volumes will be reported in nm^3. To relate the previously measured AFM volumes (in pix^2nm) to cubic nanometers, one has to simply use the fact that 1 μm ≡ 512 pixels for our instrument, under our invariant image acquisition conditions. Importantly, this change does not affect the interpretation of the results and our previous conclusions because we are simply performing a transformation from one unit of measurement to another. As before, the dynamic range of our instrument enables us to confidently identify whether UV-DDB is monomeric or dimeric in our assays. The curve was generated using the following proteins and their oligomeric states: Pot1 (65 kDa), PcrA monomer (86.4 kDa), UvrA monomer (105 kDa), Taq MutS dimer (181 kDa), UvrA dimer (210 kDa), and Taq MutS tetramer (362 kDa). The corrected calibration curve is presented in Fig. S6*B*. The fit to the data are $V(nm^3) = 1.471\ MW\ (kDa) - 7.294$ ($R^2 = 0.9886$).

7. Comparison of Kinetic Rate Constants from This Study with Previous Estimates. Bulk estimates of the kinetics of dissociation of UV-DDB from UV-damaged DNA in cellular chromatin are difficult to obtain because of the complex and unclear interaction between UV-DDB and XPC and its dependence on the ubiquitylation of each of these factors. Kinetic studies of C-terminally tagged murine DDB2-EYFP in XP20MA cells (XP-C cells) revealed a half-life of 110 s for dissociation from UV-damaged chromatin (17). Previous biochemical analysis of the dissociation kinetics of recombinant UV-DDB from photoproducts were found to be lesion dependent with a slow off rate for a high affinity lesion such as the (6–4) photoproduct ($8.1 \times 10^{-4}\ s^{-1}$) and faster off-rates for the Dewar isomer of the (6–4) photoproduct and T[t,s]T (2.9×10^{-3} and $3.7 \times 10^{-3}\ s^{-1}$, respectively) and even faster off-rates for the dissociation from T[c,s]T photoproducts ($4.6 \times 10^{-2}\ s^{-1}$) (18). However, in these studies the estimated rate constants represent the dissociation rates of a heterogeneous, unsynchronized population from not just the site-specific lesion, but also end binding, irrespective of the oligomeric state of UV-DDB bound to the DNA substrate or in the presence of other interacting partners or posttranslational modifications that may influence these estimates.

1. Wittschieben BO, Iwai S, Wood RD (2005) DDB1-DDB2 (xeroderma pigmentosum group E) protein complex recognizes a cyclobutane pyrimidine dimer, mismatches, apurinic/apyrimidinic sites, and compound lesions in DNA. *J Biol Chem* 280(48): 39982–39989.
2. Reichel A, et al. (2007) Noncovalent, site-specific biotinylation of histidine-tagged proteins. *Anal Chem* 79(22):8590–8600.
3. Kad NM, Wang H, Kennedy GG, Warshaw DM, Van Houten B (2010) Collaborative dynamic DNA scanning by nucleotide excision repair proteins investigated by single-molecule imaging of quantum-dot-labeled proteins. *Mol Cell* 37(5):702–713.
4. Wang H, Tessmer I, Croteau DL, Erie DA, Van Houten B (2008) Functional characterization and atomic force microscopy of a DNA repair protein conjugated to a quantum dot. *Nano Lett* 8(6):1631–1637.
5. Dunn AR, Kad NM, Nelson SR, Warshaw DM, Wallace SS (2011) Single Qdot-labeled glycosylase molecules use a wedge amino acid to probe for lesions while scanning along DNA. *Nucleic Acids Res* 39(17):7487–7498.
6. Alekseev S, et al. (2008) Cellular concentrations of DDB2 regulate dynamic binding of DDB1 at UV-induced DNA damage. *Mol Cell Biol* 28(24):7402–7413.
7. Tycon MA, Dial CF, Faison K, Melvin W, Fecko CJ (2012) Quantification of dye-mediated photodamage during single-molecule DNA imaging. *Anal Biochem* 426(1): 13–21.
8. Thompson RE, Larson DR, Webb WW (2002) Precise nanometer localization analysis for individual fluorescent probes. *Biophys J* 82(5):2775–2783.
9. Arnspang EC, Brewer JR, Lagerholm BC (2012) Multi-color single particle tracking with quantum dots. *PLoS ONE* 7(11):e48521.
10. Arnspang Christensen E, Kulatunga P, Lagerholm BC (2012) A single molecule investigation of the photostability of quantum dots. *PLoS ONE* 7(8):e44355.
11. Furda AM, Bess AS, Meyer JN, Van Houten B (2012) Analysis of DNA damage and repair in nuclear and mitochondrial DNA of animal cells using quantitative PCR. *Methods Mol Biol* 920:111–132.
12. Hughes CD, et al. (2013) Real-time single-molecule imaging reveals a direct interaction between UvrC and UvrB on DNA tightropes. *Nucleic Acids Res* 41(9):4901–4912.
13. Schurr JM (1975) The one-dimensional diffusion coefficient of proteins absorbed on DNA hydrodynamic considerations. *Biophys Chem* 9(4):413–414.
14. Geng H, et al. (2011) In vitro studies of DNA mismatch repair proteins. *Anal Biochem* 413(2):179–184.
15. Yeh JI, et al. (2012) Damaged DNA induced UV-damaged DNA-binding protein (UV-DDB) dimerization and its roles in chromatinized DNA repair. *Proc Natl Acad Sci USA* 109(41):E2737–E2746.
16. Wang H, Nora GJ, Ghodke H, Opresko PL (2011) Single molecule studies of physiologically relevant telomeric tails reveal POT1 mechanism for promoting G-quadruplex unfolding. *J Biol Chem* 286(9):7479–7489.
17. Luijsterburg MS, et al. (2007) Dynamic in vivo interaction of DDB2 E3 ubiquitin ligase with UV-damaged DNA is independent of damage-recognition protein XPC. *J Cell Sci* 120(Pt 15):2706–2716.
18. Reardon JT, et al. (1993) Comparative analysis of binding of human damaged DNA-binding protein (XPE) and Escherichia coli damage recognition protein (UvrA) to the major ultraviolet photoproducts: T[c,s]T, T[t,s]T, T[6-4]T, and T[Dewar]T. *J Biol Chem* 268(28):21301–21308.

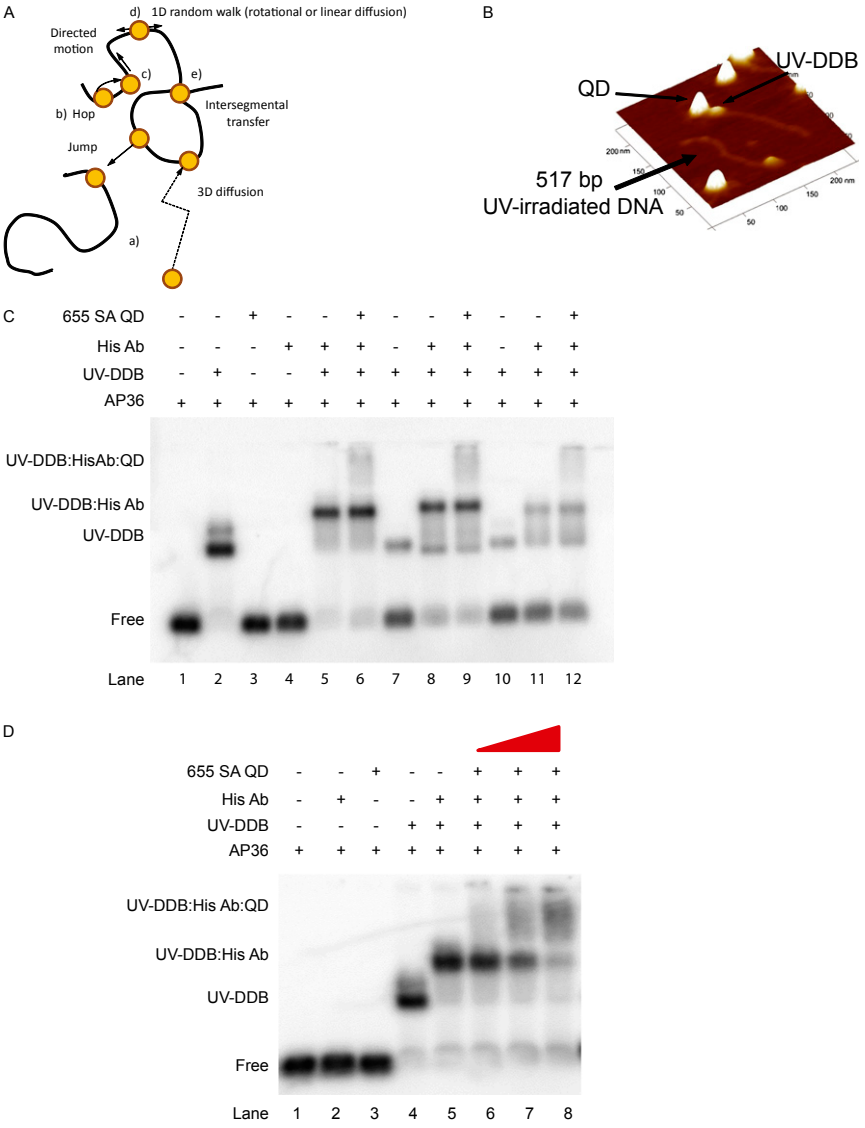

Fig. S1. Related to Fig. 1. (*A*) Search modes used by DNA-binding proteins (yellow circles) to locate their target sequences including (a) 3D diffusion and jumping, (b) hopping, (c) directed motion, (d) 1D diffusion, and (e) intersegmental transfer. (*B*) AFM image (250 nm × 250 nm × 3 nm) with 3D rendering, showing goat anti-mouse IgG-coated QDs colocalized to UV-irradiated 517-bp PCR product in the presence of the anti-FLAG antibody conjugated to $^{FLAG\text{-}His}$DDB1-DDB2. (*C*) Agarose EMSA showing that 5′ ^{32}P-labeled 36-mer containing AP site (lane 1) can be bound by UV-DDB (lane 2). Lanes 3 and 4 are negative controls indicating that neither the His-Ab nor the QD nonspecifically bind the 36-mer DNA substrate. Lane 5 indicates a complete shift in the presence of His-Ab and lane 6 indicates a supershift in the presence of SA-QD. For these experiments, 2.5 nM dsDNA AP36 substrate containing an abasic site was incubated with either UV-DDB only ($^{FLAG\text{-}His}$DDB1/DDB2, 50 nM; ^{His}DDB1/^{FLAG}DDB2, 29 nM; and DDB1/$^{FLAG\text{-}His}$DDB2, 37 nM in lanes 2, 7, and 10, respectively) and penta-His Ab [UV-DDB:penta-His Ab = 1:5 in lanes 5, 8 and 11, respectively) and 655 nm SA-QDs (UV-DDB:QDs = 1:1 in lanes 6, 9, and 12, respectively). (*D*) Agarose EMSA showing 5′ ^{32}P-labeled 36-mer containing an AP site (2.5 nM), alone (lane 1), or in the presence of His-Ab (lane 2), or 655 SAQD (lane 3), or incubated with $^{FLAG\text{-}His}$DDB1/DDB2 (lane 4) and antibody (lanes 5–8) and QD (lanes 6–8) ratios were varied as indicated in the lanes keeping UV-DDB concentration constant (lane 6, UV-DDB:Ab:QD = 1:5:1; lane 7, UV-DDB:Ab:QD = 1:5:2.5; and lane 8, UV-DDB:Ab:QD = 1:5:5). Red triangle indicates increasing concentration of QD.

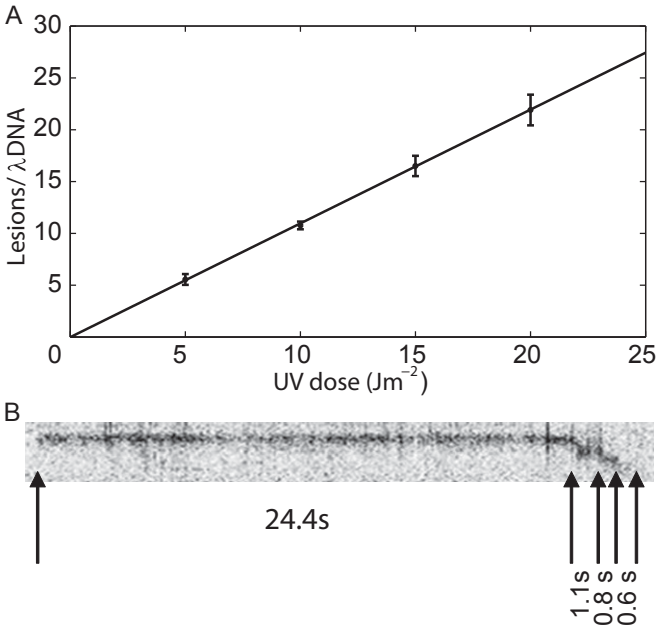

Fig. S2. Related to Fig. 2. (*A*) UV-induced photoproduct frequency per λ-DNA is a linear function of UV dose as measured by qPCR. (*B*) Kymograph of UV-DDB jumping between vicinal DNA molecules in the field of view.

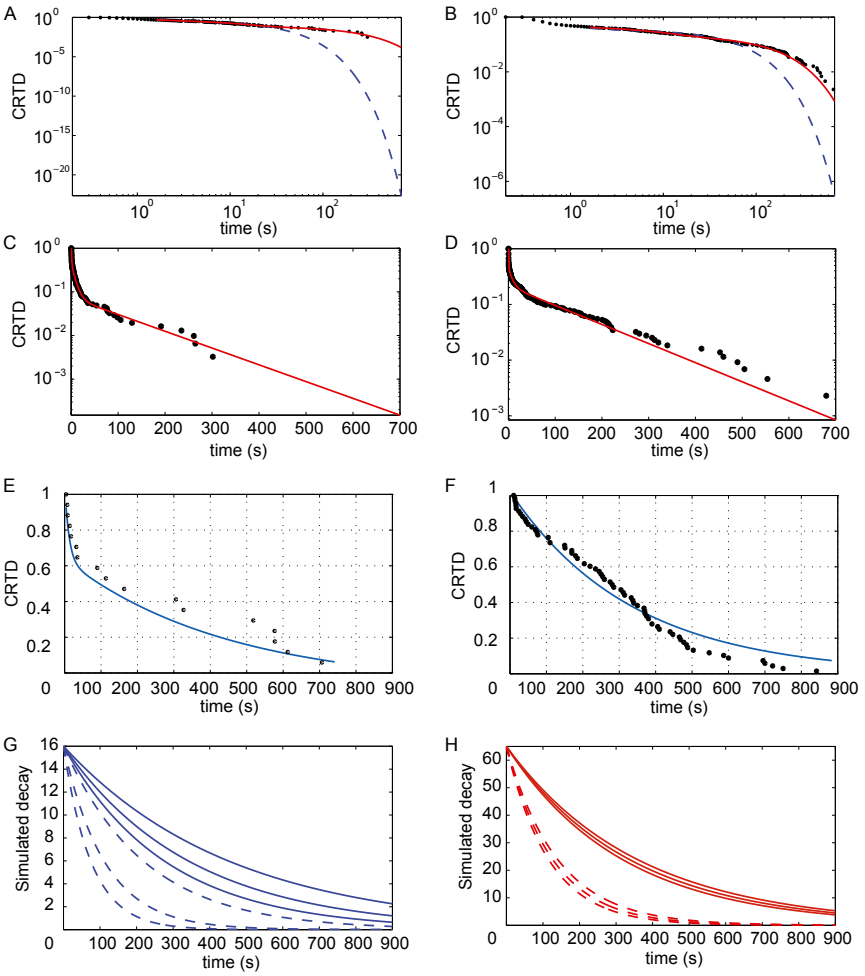

Fig. S3. Related to Fig. 3. Log-Log plot of CRTD vs. time for WT UV-DDB interacting with (*A*) undamaged DNA (Movie S1) and (*B*) UV-damaged DNA (Movie S2) in low-salt buffer. Log-linear plot of CRTD vs. time for WT UV-DDB interacting with (*C*) undamaged DNA (Movie S1) and (*D*) UV-damaged DNA (Movie S2) in low-salt buffer. Black circles represent experimental data. Double and triple exponential fits are shown in dashed blue and solid red lines, respectively. CRTD vs. *t* plot for dissociating UV-DDB from (*E*) undamaged DNA and (*F*) UV-damaged DNA with exponential fits (blue) to the experimental data (black circles). *G* and *H* represent simulated decay for dissociating UV-DDB from undamaged and UV-damaged DNA, respectively, according to the Poisson processes, T_3 (dashed) or T_4 process (solid), using the estimated time constant (τ) and the upper and lower bound estimates (Tables 1 and 2).

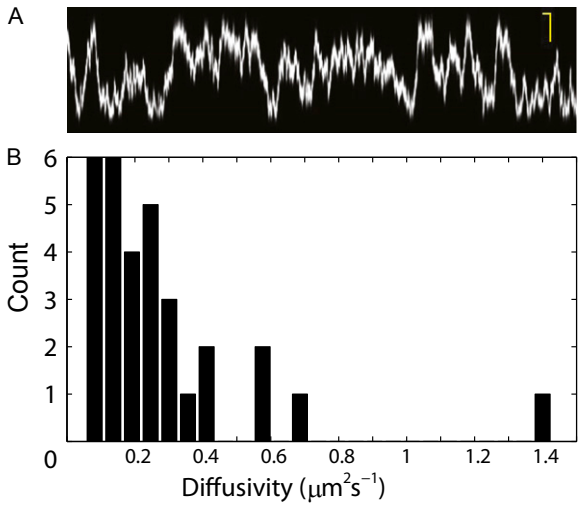

Fig. S4. Related to Fig. 2. (*A*) Representative kymograph of UV-DDB sliding on DNA in high-salt buffer (Movie S3). (*B*) Histogram of diffusion constants for UV-DDB sliding on DNA at high ionic strength. [Horizontal scale bar: 1 s; vertical scale bar: 2 μm (n = 31).]

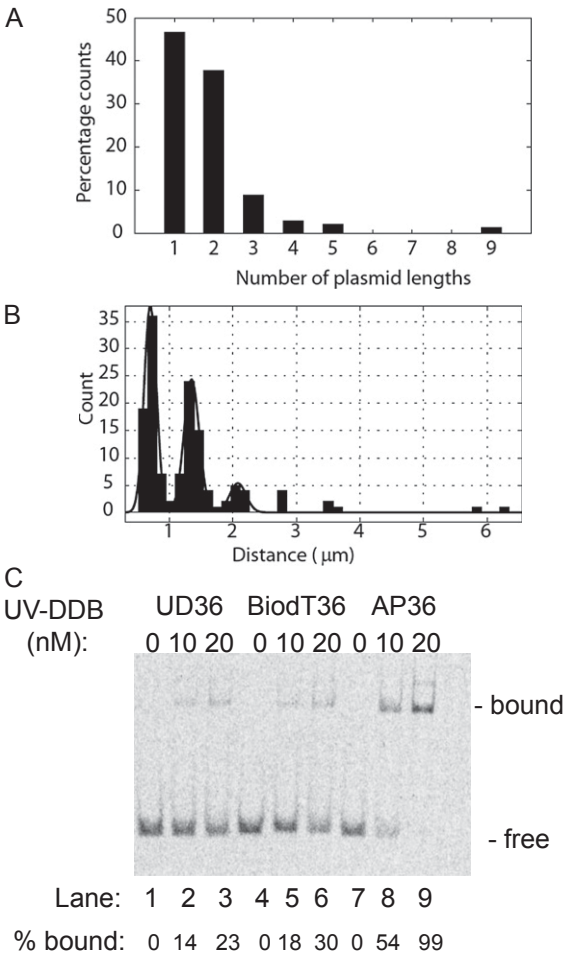

Fig. S5. Related to Fig. 4. (*A*) Histogram of the percentage counts of the distance (normalized to linearized DNA length before ligation) between adjacent QDs on a DNA tightrope containing an abasic site analog at a defined site. (*B*) Gaussian fit to the histogram of measured distances between adjacent QDs on DNA substrate. (*C*) Electrophoretic mobility shift assay demonstrating binding of UV-DDB to 36-mer DNA that is undamaged (UD36, lane 1), or contains the biodT lesion (bio36, lane 4) or DNA containing an abasic site (AP36, lane 7). Addition of UV-DDB at 10 nM results in weak binding to UD36 (lane 2) and bio36 (lane 5) and strong binding to AP36 (lane 8). At 20 nM UV-DDB, binding to UD36 (lane 3) and bio36 (lane 6) substrates increases modestly, however, the AP36 substrate is completely bound by UV-DDB (lane 9).

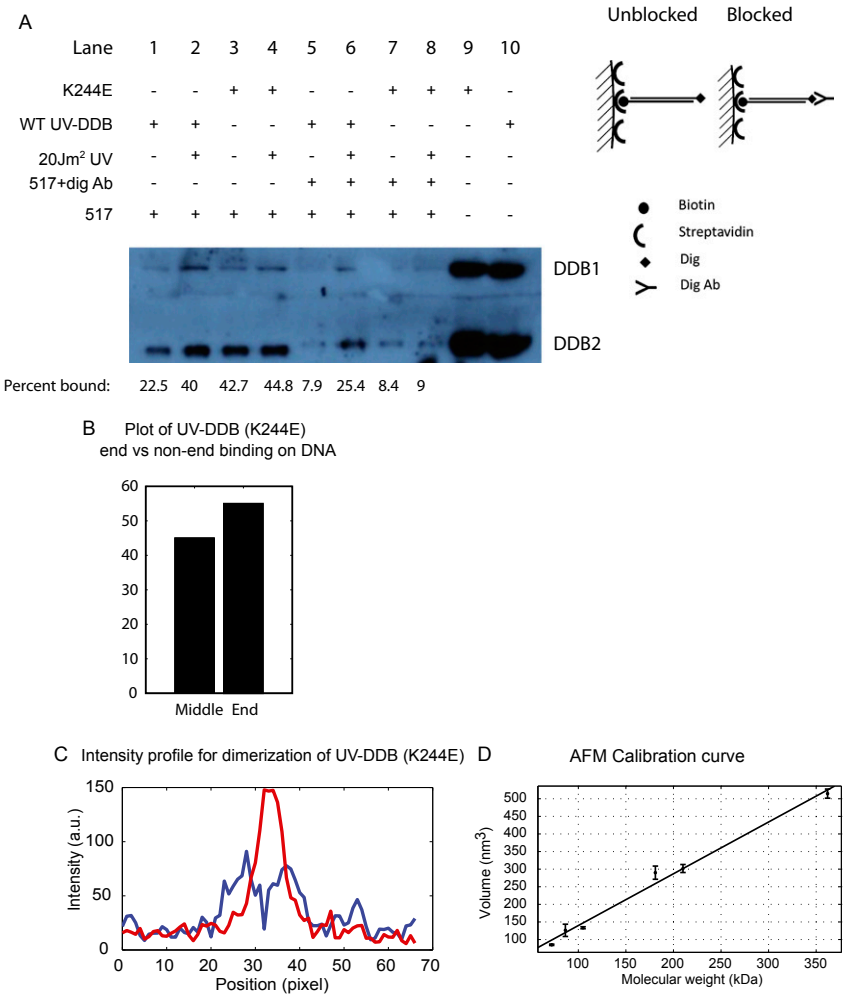

Fig. S6. Related to Fig. 5. (*A*) Western blot assay for binding of WT UV-DDB and UV-DDB (K244) to damaged or undamaged DNA with blocked (Dig-Ab/biotin-SA) or one free end (in the absence of Dig-Ab). (*B*) Plot of end vs. nonspecific binding of UV-DDB (K244E) on 517-bp undamaged DNA. (*C*) Intensity profile of dimerizing UV-DDB (K244E) before collision (blue) and after dimerization (red) (Movie S7). (*D*) AFM calibration curve relating the molecular weight of a complex to its measured AFM volume, mean ± SD of three separate determinations.

Table S1. Fitting parameters for double or triple exponential fits to CRTDs of transient UV-DDB on undamaged or UV-damaged DNA

	$N_p = 2$				$N_p = 3$			
Type of DNA	df	R^2	SSE	SSE/df	df	R^2	SSE	SSE/df
Undamaged DNA	343	0.9929	3.82E-02	1.11E-04	341	0.9972	1.61E-02	4.72E-05
UV-damaged DNA	639	0.9658	1.59E-01	2.49E-04	637	0.9938	2.91E-02	4.57E-05

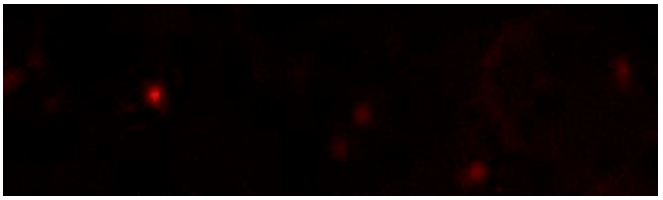

Movie S1. Related to Fig. 1. Movie of QD UV-DDB jumping between vicinal DNA molecules in a web of undamaged λ-DNA suspended between beads in low-salt buffer. Here, 30 s of video are played back at 15 fps.

Movie S1

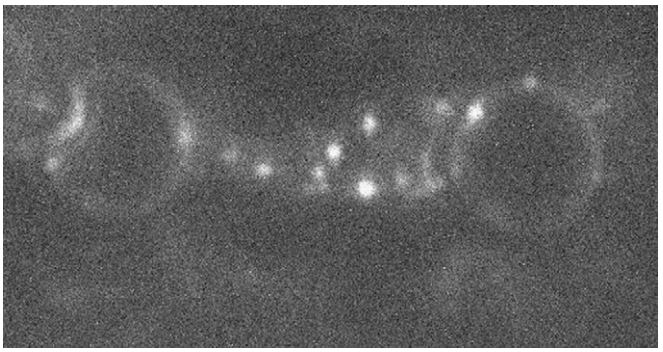

Movie S2. Related to Fig. 2. Movie of QD UV-DDB complexes bound to UV-damaged DNA in low-salt buffer. Here, 15 min of video are played back at 15 fps.

Movie S2

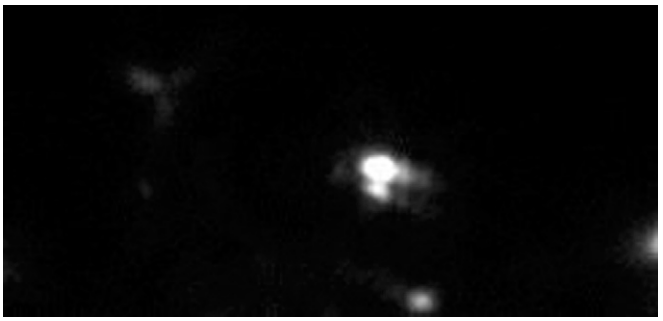

Movie S3. Related to Fig. 2. Movie of QD UV-DDB sliding on DNA tightrope in high-salt buffer. Here, 2 min of video are played back at 15 fps.

Movie S3

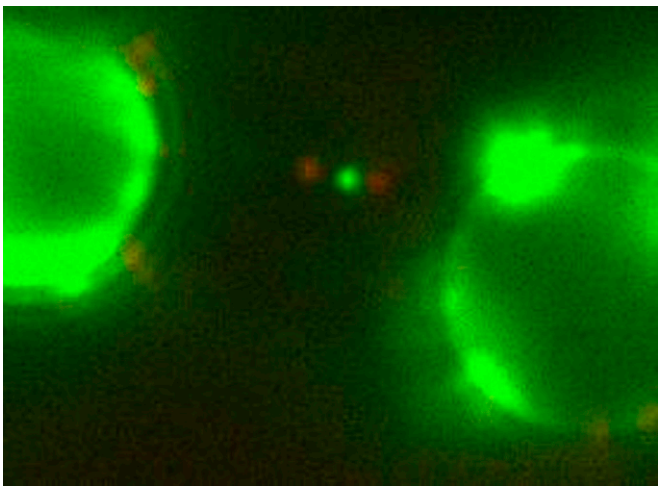

Movie S4. Related to Fig. 4. Movie of QD UV-DDB (red) colocalized to sites of lesions on APbiodT (green) substrate in low-salt buffer. Here, 15 min of video are played back at 15 fps.

Movie S4

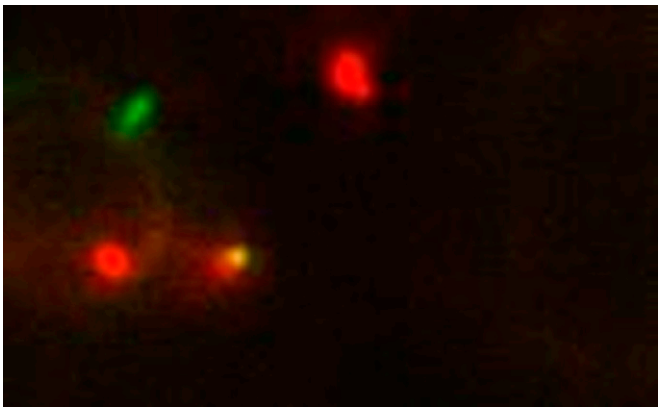

Movie S5. Related to Fig. 4. Movie of colocalized green UV-DDB with red UV-DDB on UV-damaged DNA tightropes in low-salt buffer. Here, 15 min of video are played back at 15 fps.

Movie S5

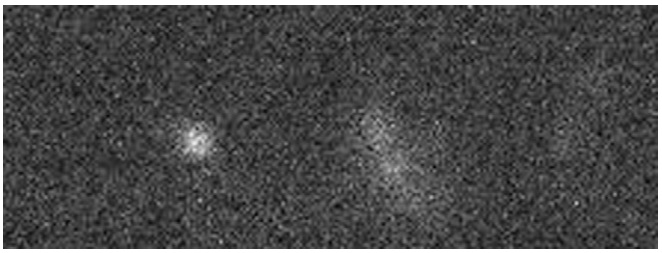

Movie S6. Related to Fig. 5. Movie of UV-DDB (K244E) sliding on AP-biodT DNA in low-salt buffer. Here, 2 min of video are replayed at 30 fps.

Movie S6

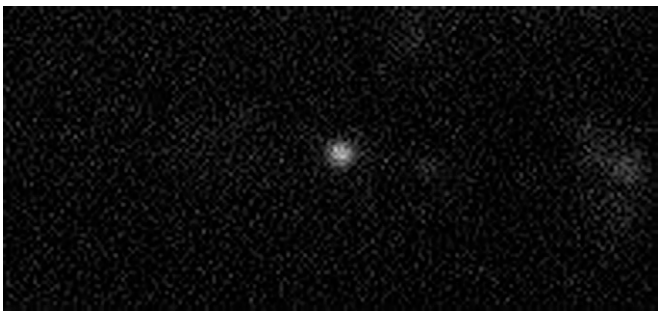

Movie S7. Related to Fig. 5. Movie of UV-DDB (K244E) dimerizing on undamaged λ-DNA tightropes in low-salt buffer.

Movie S7

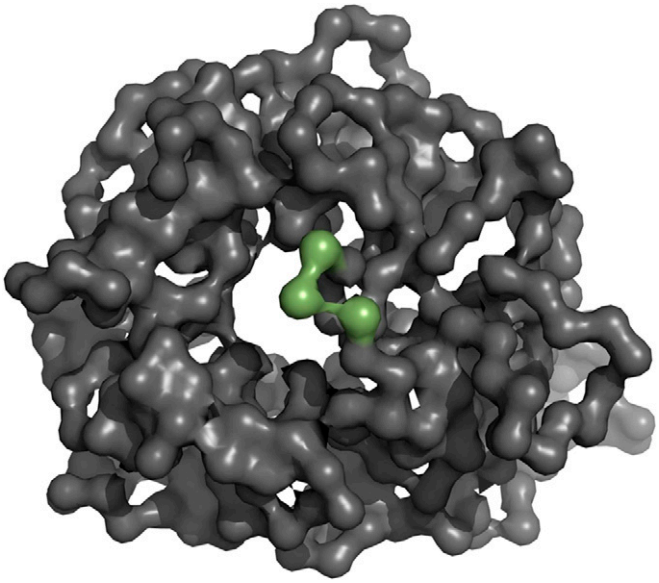

Movie S8. Related to Fig. 6. Movie of predicted conformational changes in DDB2 from anisotropic network model of DDB2. Green represents FQH domain.

Movie S8